Correlation of aerosol nucleation rate with sulfuric acid and ammonia in Kent, Ohio: An atmospheric observation

Mark E. Erupe,[1] David R. Benson,[1] Jingmin Li,[1] Li-Hao Young,[1,2] Bart Verheggen,[3] Mohammed Al-Refai,[1] Omar Tahboub,[1] Victoria Cunningham,[1] Flavia Frimpong,[1] Albert A. Viggiano,[4] and Shan-Hu Lee[1]

Received 4 February 2010; revised 30 June 2010; accepted 21 July 2010; published 10 December 2010.

[1] New particle formation (NPF) occurs in various atmospheric environments, and these newly formed particles have the potential to grow to cloud condensation nuclei. But at present it is unclear which chemical species are involved in aerosol nucleation and growth, in part because there are only a limited number of simultaneous measurements of aerosol precursors and aerosol size distributions. Observations of ambient aerosol size distributions, sulfuric acid, and ammonia were made for over a year in Kent, Ohio, a relatively less polluted continental environment. Particle sizes in the diameter range from 3 to 1000 nm were measured continuously through the whole year, while sulfuric acid and ammonia were measured seasonally with two chemical ionization mass spectrometers. Strong NPF events were more frequently found during the spring and fall and less frequently during the summer and winter. The median of measured sulfuric acid was higher in spring (5.2×10^6 cm^{-3}) and summer (2.9×10^6 cm^{-3}) than in winter (6×10^5 cm^{-3}) and fall (5×10^5 cm^{-3}). We have used the inverse model Particle Growth and Nucleation to derive aerosol nucleation and growth rates from the measured aerosol size distributions. Nucleation rates derived during the NPF events ranged from 1.4 to 12.9 cm^{-3} s^{-1} and were proportional to the measured sulfuric acid concentration with a power of 0.6–2.3. Our results show that sulfuric acid is an important aerosol nucleation precursor, but only a small fraction of the aerosol growth rates could be explained by the condensation of sulfuric acid alone. Ammonia mixing ratios did not have a diurnal trend but had some seasonal variations, higher in spring than in fall and winter, typically at sub-ppbv level; aerosol nucleation rates did not show a clear correlation with ammonia at least at this sub-ppbv level, mostly because the ammonia mixing ratios were nearly constant. Our observations also indicate that the role that ammonia plays in aerosol nucleation is more complicated than is currently understood by the aerosol nucleation theories.

Citation: Erupe, M. E., et al. (2010), Correlation of aerosol nucleation rate with sulfuric acid and ammonia in Kent, Ohio: An atmospheric observation, *J. Geophys. Res.*, *115*, D23216, doi:10.1029/2010JD013942.

1. Introduction

[2] Atmospheric aerosols affect human health and global climate, and it is important to understand the processes which influence their number concentrations. Such processes include formation and growth of aerosol particles. New particle formation (NPF) has been observed all over the world under a wide range of atmospheric conditions [*Kulmala et al.*, 2004] and these newly formed particles can grow to cloud condensation nuclei (CCN). However, the nucleation and growth mechanisms are poorly understood and it is even unclear which chemical species are involved in the nucleation processes. This is in part due to the limited number of studies that simultaneously measured aerosol sizes and gas-phase precursors such as sulfuric acid (H_2SO_4), ammonia (NH_3), and organic compounds. Because nucleation is a nonlinear process and nucleation rates are extremely sensitive to aerosol precursor concentrations [*Kerminen and Wexler*, 1996; *Lee et al.*, 2003], it is important to directly measure aerosol precursors in order to correctly predict aerosol formation rates and number concentrations.

[3] H_2SO_4 is an important aerosol precursor [*Ball et al.*, 1999; *Benson et al.*, 2008; *Young et al.*, 2008; *Zhang et al.*, 2009], because of its low vapor pressure (e.g., 1.88×10^{-2} Pa at 25°C [*Seinfeld and Pandis*, 2006]) and its unique

[1]Department of Chemistry, Kent State University, Kent, Ohio, USA.
[2]Department of Occupational Safety and Health, China Medical University, Taichung, Taiwan.
[3]Department of Air Quality and Climate Change, Energy Research Centre of the Netherlands, Petten, Netherlands.
[4]Air Force Research Laboratory, Hanscom Air Force Base, Bedford, Massachusetts, USA.

0148-0227/10/2010JD013942

ability to form clusters in the atmosphere. Previous atmospheric observations of H_2SO_4 and NH_3 made for NPF studies are summarized in Table 1. H_2SO_4 concentrations ($[H_2SO_4]$) were usually measured with the chemical ionization mass spectrometer (CIMS) technique [*Eisele and Tanner*, 1993]. P. H. McMurry and his colleagues have made early studies of NPF in connection with measured $[H_2SO_4]$ under various atmospheric conditions, for example, in Mauna Loa and Idaho Hill, and in the free troposphere during PEM-WEST and ACE-1 missions [*Weber et al.*, 1997, 1998, 1999]. Typical noon time peak $[H_2SO_4]$ in the 10^6–10^7 cm^{-3} range was reported at these sites and based on these $[H_2SO_4]$ values, they concluded that their measured particle concentrations are much higher than those predicted from the classical homogeneous nucleation of sulfuric acid. More recent work from the same group, in collaboration with other colleagues, made in Atlanta, GA, Boulder, CO, Tecamac, Mexico, and Macquarie Island, Australia, have focused on the numerical relationship of nucleation rates (J) and $[H_2SO_4]$ [*Kuang et al.*, 2008; *McMurry and Eisele*, 2005; *McMurry et al.*, 2005]. Long-term measurements of H_2SO_4 have been made also in Europe, including Hyytiälä [*Dal Maso et al.*, 2005; *Fiedler et al.*, 2005; *Sihto et al.*, 2006], Heidelberg [*Fiedler et al.*, 2005] and Hohenpeissenberg [*Birmili et al.*, 2000, 2003; *Paasonen et al.*, 2009]. These observations also showed that $[H_2SO_4]$ values typically were at the 10^6–10^7 cm^{-3} range at noon, depending on the season. There are also measurements that have shown that $[H_2SO_4]$ can be at the 10^8 cm^{-3} range in the polluted environment [*Bardouki et al.*, 2003; *Berresheim et al.*, 2002]. While these studies were mostly ground-based or in the boundary layer, H_2SO_4 measurements also exist for the free troposphere [*Clarke et al.*, 1998; *Weber et al.*, 1998] and for the upper troposphere and lower stratosphere [*Lee et al.*, 2003].

[4] Atmospheric observations often showed that the observed nucleation rates are much higher than those predicted from the H_2SO_4-H_2O binary homogeneous nucleation (BHN) theory and growth rates (GR) derived from H_2SO_4 condensation are also much smaller than those derived from the measured aerosol size distributions [*Birmili et al.*, 2003; *Dal Maso et al.*, 2005; *Fiedler et al.*, 2005; *Kuang et al.*, 2008; *Kulmala et al.*, 2004; *McMurry et al.*, 2005; *Paasonen et al.*, 2009; *Riipinen et al.*, 2007; *Sihto et al.*, 2006; *Stolzenberg et al.*, 2005; *Weber et al.*, 1996]. GR is an important parameter which determines whether these newly formed nanometer size particles can effectively grow to cloud condensation nuclei sizes (>40 nm) before they are scavenged by preexisting particles. For most of the time, GR values calculated from the measured $[H_2SO_4]$ were often 1 order of magnitude lower than those derived from measured aerosol sizes, suggesting that condensable species other than H_2SO_4 may also be involved in aerosol growth.

[5] Among other potential aerosol nucleation precursors, NH_3 has been considered to play an important role via ternary homogeneous nucleation (THN) or multicomponent nucleation process [*Kulmala et al.*, 2002; *Merikanto et al.*, 2007; *Napari et al.*, 2002]. NH_3 is ubiquitous and the major gas phase base in the atmosphere. Tropospheric NH_3 mixing ratios ($[NH_3]$) range from several parts per trillion by volume (pptv) up to several hundreds ppbv and sometimes even up to several hundreds ppmv levels [*Gilliland et al.*, 2003; *Herndon et al.*, 2005; *Huai et al.*, 2003; *Li et al.*, 2006; *Nowak et al.*, 2007], depending on the proximity to emission sources, altitude, and acidity of aerosol particles in the atmosphere. NH_3 can lower the partial pressure of H_2SO_4 vapor above the solution surface [*Scott and Cattell*, 1979] and therefore, can enhance nucleation rates of H_2SO_4 particles, as demonstrated by laboratory observations [*Ball et al.*, 1999; *Benson et al.*, 2009]. Chemical composition studies in Atlanta, GA also revealed that newly formed nanometer particles contain ammonium and sulfate ions [*Smith et al.*, 2005]. Global aerosol modeling predictions suggest that THN involving NH_3 is the dominant nucleation mechanism in the troposphere and lower stratosphere [*Lucas and Akimoto*, 2006]; note, this cited study has also used the earlier version of NH_3-THN parameterization [*Napari et al.*, 2002] which overpredicts aerosol nucleation rates. Regional aerosol microphysical modeling studies also showed that NH_3-THN can be used to explain most nucleation events found in the eastern United States [*Gaydos et al.*, 2005; *Jung et al.*, 2006, 2008; *Stanier et al.*, 2004]; these calculations also used NH_3-THN parameterization [*Napari et al.*, 2002]. Using an aerosol dynamic model, Kulmala and coworkers have also shown that NH_3-THN can be used to simulate the production of high concentrations of thermodynamically stable clusters (<3 nm) in certain atmospheric conditions [*Kulmala et al.*, 2002].

[6] Despite the importance and unique role of NH_3 in nucleation, simultaneous observations of NH_3, H_2SO_4 and aerosol size distributions are surprisingly scarce (Table 1), and such a lack of measurements makes it hard to quantify the role of NH_3 in atmospheric nucleation. These kinds of measurements were made in Atlanta, GA [*McMurry and Eisele*, 2005; *McMurry et al.*, 2005; *Nowak et al.*, 2006], where both H_2SO_4 [*Eisele and Tanner*, 1993] and NH_3 [*Nowak et al.*, 2006] were measured by two CIMSs. The Atlanta measurements highlighted the importance of NH_3 in aerosol formation and growth processes. In other NPF studies involving NH_3 measurements, NH_3 was often detected with techniques that have longer time response (over several hours) compared to CIMS (several seconds). For example, at a study site on Mt. Norikura in Japan NH_3 was measured using an acid-impregnated filter and found no positive correlation between $[NH_3]$ and NPF for NH_3 at the sub-ppbv level [*Nishita et al.*, 2008]. Other NH_3 measurements for NPF studies include the Hyytiälä measurements with a refluxing mist chamber [*Riipinen et al.*, 2007].

[7] Here we show atmospheric observations of aerosol size distributions, H_2SO_4 and NH_3 made in Kent, Ohio, over a period of one year. Particle measurements were made in the size range from 3 to 1000 nm starting from January 2006 to the present, continuously. H_2SO_4 and NH_3 were measured with two CIMSs on seasonal basis starting from summer of 2008. To our knowledge, this is the first time that seasonal variation of these two major nucleation precursors has been measured simultaneously, together with aerosol size distributions. We applied the inverse model Particle Growth and Nucleation (PARGAN), which is different from those used in most previous NPF studies, to calculate nucleation rate (J) and growth rate (GR) [*Verheggen*, 2004; *Verheggen and Mozurkewich*, 2006]. The purpose of the present study is to determine the actual connection between J and GR with the measured $[H_2SO_4]$ and $[NH_3]$ from the

Table 1. Summary of NPF Studies That Had Simultaneous Measurements of H_2SO_4 or NH_3[a]

Location (Platform)	Date	$[H_2SO_4]$[b] (10^6 cm^{-3})	$[NH_3]$ (ppbv)	GR[c] (nm h^{-1})	J (cm^3 s^{-1})	Log C	P	References
Hohenpeissenberg, Germany (ground)	1998–2000	5.57–10.29	NR	2.6	0.01–9	−6.8 to −13.5	1–2	*Birmili et al.* [2003] and *Paasonen et al.* [2009]
Heidelberg, Germany (ground)	Feb–Apr 2004	2.2–6.3	NR	2.1–22.9	0.65–5.95	−5.0 to −11.4	1–2	*Fiedler et al.* [2005] and *Riipinen et al.* [2007]
Hyyttiala, Finland (ground)	Mar–Apr 2003, Apr–May 2005, Mar–Jun 2007	0.6–7.6, 0.1–10, 0.3–2	NR, 0.04–4,[d] NR	1.7–12.2, 0.6–10, 1.9–4.2	0.1–6.97, 0.2, 0.65	−6.0 to −12.3, −6.6 to −13.5, −6.7 to −12.9	1–2, 1–2, 1–2	*Fiedler et al.* [2005], *Riipinen et al.* [2007], *Sihto et al.* [2006], *Manninen et al.* [2009], *Nieminen et al.* [2009], and *Petäjä et al.* [2009]
Mace Head, Ireland (ground)	Jun 1999	2–120	0.02–2[e]	36–1260	10^4–10^6	NR	NR	*Berresheim et al.* [2002], *Kulmala et al.* [2002], and *O'Dowd et al.* [2002]
Atlanta, Georgia (ground)	Aug 2002	10–100	0.4–13[b]	2.86–22.02	NR	−13.9	2.01	*Kuang et al.* [2008], *Kuang and McMurry* [2010], *McMurry et al.* [2005], and *Stolzenberg et al.* [2005]
Idaho Hill, Colorado (ground)	Sep 1993	8.4–9.8	NR	0.5–2	1	NR	NR	*Kuang et al.* [2008], *Kuang and McMurry* [2010], and *Weber et al.* [1997, 1999]
Mauna Loa, Hawaii (ground)	Jun–Jul 1992	7.8–9.5	NR	0.1–0.4	0.5	NR	NR	*Kuang et al.* [2008], *Kuang and McMurry* [2010], and *Weber et al.* [1996, 1999]
Boulder, Colorado (ground)	Sep 2004	1–40	NR	3.5–9.7[f]	2.4[g]	−13.3	1.98	*Eisele et al.* [2006], *Iida et al.* [2006], *Kuang et al.* [2008], and *Kuang and McMurry* [2010]
Tecamac, Mexico (ground)	Mar 2006	30–80	NR	15–40	1900–3000	−12.2	1.99	*Iida et al.* [2008], *Kuang et al.* [2008], *Kuang and McMurry* [2010], and *Smith et al.* [2008]
Macquarie Island, Australia (aircraft)	Nov–Dec 1995	4.4–7.3	NR	2–5	0.5–10	−14.0	2.00	*Kuang et al.* [2008], *Kuang and McMurry* [2010], and *Weber et al.* [1998, 1999]
Kent, Ohio (ground)	2008–2009	0.7–5.2	0.05–0.5[b]	2.5–11.7	1.2–12.9	−3.2 to −17.2	0.6–2.3	this work

[a]Some of these measurements may include long-term measurements of aerosol size distributions, like this study in Kent, Ohio, but here we included only the measurement periods that also had either H_2SO_4 and/or NH_3. NR indicates that data were not reported.
[b]Measurements were made using CIMS.
[c]*GR* was derived from particle size distribution (unless otherwise stated).
[d]Measurements were made using refluxing mist chamber.
[e]Measurements were made using diffusion scrubber.
[f]*GR* was derived from the time-shift method.
[g]Value for one event day.

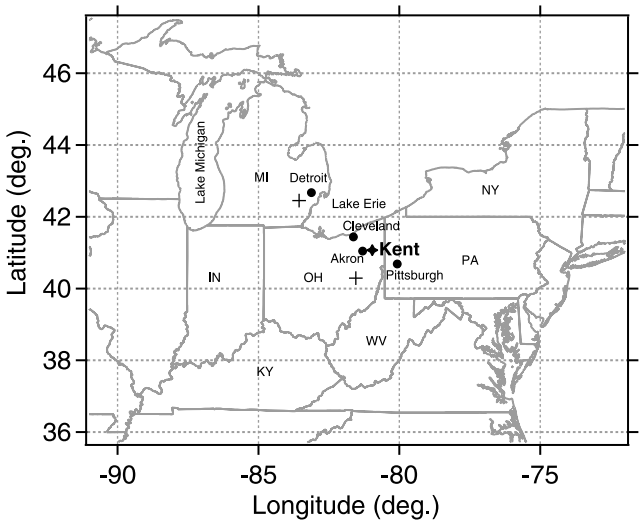

Figure 1. A regional map showing the location of Kent, Ohio (black star), including major nearby urban areas (black circles). The pluses are the sites of two large power plants (SO_2 sources) in this region.

atmospheric observation in this new location using an independent inversion model and to compare with other NPF studies. A second manuscript discusses the effects of meteorological conditions on NPF from statistical analysis of long-term measurements (~4 years) of aerosol sizes in Kent (L.-H. Young et al., Investigation of the effects of meteorological conditions on particle formation in Kent, Ohio: Long-term ground based observation of new particle formation, manuscript in preparation, 2010).

2. Observation Methods

2.1. Observation Site and Measurement Period

[8] Aerosol size distributions and number concentrations have been measured continuously in Kent, Ohio, since January 2006. H_2SO_4 concentrations ([H_2SO_4] in the unit of cm^{-3}) and NH_3 mixing ratios ([NH_3] presented in pptv in this study to be consistent with NH_3-THN models [*Merikanto et al.*, 2007]; 1 pptv $\approx 2 \times 10^7$ cm^{-3}) have also been measured with CIMS since August 2008 on seasonal basis. The sampling site is located at the top floor of Williams Hall (15 m above the ground level) on the main campus of Kent State University (41.15° N, 81.36° W). Kent is a small college town with a population of about 30,000, located in Northeastern Ohio. Kent is relatively rural itself, but is also surrounded by three urban cities, about 40 miles southeast of Cleveland, about 15 miles east of Akron, and about 100 miles west from Pittsburgh, PA (Figure 1). The weather in Ohio is humid, especially in summer. Northeastern Ohio is also known for its haze and gray colored sky in winter. Northeastern Ohio has rich vegetation with numerous large forests (maple-beech-birch) and has many natural lakes. Ohio is also one of the states that currently suffer from air pollution problems, failing to attain the National Ambient Air Quality Standards (NAAQS) for ozone and $PM_{2.5}$ (particulate matter smaller than 2.5 μm) (http://www.epa.gov/air/airtrends/pm.html). It is noted that SO_2 emission in Ohio ranks among the top in the nation (http://www.epa.gov/air/sulfurdioxide/) because of the strong SO_2 emission from large size coal-burning power plants in the great lakes area, such as Detroit Monroe Power Plant (Monroe County, Michigan) and Conesville Power Plant (Coshocton, Ohio) (Figure 1); typically, the reported SO_2 concentrations were nearly at the ppbv or tens of ppbv range year around in Akron and Cleveland in recent years.

[9] Because of the combination of its relatively low surface areas of aerosol particles compared to typical EPA supersites (extremely polluted) where most of NPF studies were made previously [*McMurry et al.*, 2005; *Stanier et al.*, 2004], active vegetation (organic and NH_3 emissions), and possible transport of aerosol precursors from the surrounding urban and industrialized areas, Kent is an ideal location for NPF studies. Ultrafine particles measured in Kent may be formed locally via nucleation processes or transported from nearby urban cities where they are also directly emitted from industrial plumes or fossil fuel combustion and automobile sources. Data from this new measurement site can be also compared with other NPF studies made at different environments, including very polluted EPA supersites (such as Pittsburg, PA and Atlanta, GA) [*Kuang et al.*, 2008; *McMurry and Eisele*, 2005; *Stanier and Solomon*, 2006; *Verheggen and Mozurkewich*, 2002], can provide new insights into aerosol formation processes.

2.2. Instruments

2.2.1. Particle Measurements

[10] Particles were sampled continuously from a near isokinetic, laminar flow aerosol sampling inlet with an electrically grounded stainless steel inlet. Three types of Scanning Mobility Particle Sizer (SMPS) (TSI, St Paul, MN) systems were used. These were butanol-based TSI3085/3776 (in the size range from 3 to 170 nm), TSI3081/3772 (size range: 17–1000 nm) and the water-based TSI3085/3786 (3–102 nm), which together provide a combined size range of 3–1000 nm, the typical atmospheric aerosol size range. During the spring of 2009, all three instruments were operated simultaneously, while two were operated simultaneously during other periods (typical combination of TSI3085/3776 and TSI 3081/3772). On the basis of our sampling inlet dimension, we estimated ultrafine particle losses in the sampling lines (primarily due to diffusion) to be <20%, which would not contribute significantly to the measured particle number concentrations.

[11] By comparing the number concentrations of small particles in the size range from 3 to 25 nm (N_{3-25}) measured with the water-CPC (condensation particle counter) and butanol-CPC, we also tried to indirectly probe the composition of nucleated species. From our previous laboratory studies of H_2SO_4-H_2O BHN, we found that there is a nearly linear relation between particle concentrations measured by water-CPC and butanol-CPC for pure H_2SO_4 particles in the size range from 3 to 10 nm; water-CPC concentrations are higher than butanol-CPC concentrations for H_2SO_4 particles, compared to that derived from ambient aerosols [*Young et al.*, 2008]. Thus, the ratio of particle concentrations measured with water- and butanol-CPC can be used for indirect analysis of aerosol chemical composition of newly formed particles and provide a further insight into the species involved in growth of these freshly nucleated particles.

2.2.2. H_2SO_4-CIMS

[12] Gas phase H_2SO_4 concentrations were measured by a chemical ionization mass spectrometer (CIMS) [*Benson et al.*, 2008; *Eisele and Tanner*, 1993; *Young et al.*, 2008]. The sampling inlet uses a high flow rate (~4 L per minute) to minimize wall loss of H_2SO_4 in the inlet, as adopted from *Sjostedt et al.* [2007]. To detect H_2SO_4, NO_3^- reagent ions are used in the CIMS. Sulfuric acid was measured with the following ion-molecule reaction [*Eisele and Tanner*, 1993; *Viggiano et al.*, 1982, 1997]:

$$NO_3^- + H_2SO_4 \rightarrow HSO_4^- + HNO_3. \quad \text{(R1)}$$

HNO_3 is added into the stream of sheath air, and ionized upon encounter with electrons produced by the ^{210}Po ionization source. We monitor HSO_4^- (97 amu) and NO_3^- (62 amu) (Figure 2a) and use their ratios to calculate $[H_2SO_4]$ on the basis of the following equation:

$$[H_2SO_4] \approx \frac{HSO_4^-}{[NO_3^-]\kappa t}. \quad (1)$$

Here, $[HSO_4^-]$ and $[NO_3^-]$ are ion count rates (Hz) (only relative concentrations of the ions matter), k is the reaction rate constant (2.32×10^{-9} cm^3 s^{-1}) [*Viggiano et al.*, 1997], and t is the ion-molecule reaction time (typically 0.1 s in this study). The detection limit of H_2SO_4-CIMS was ~2×10^5 cm^{-3} and the uncertainty associated with our ambient measurements was estimated to be ~60% at maximum. Longer averaging times were used in data analysis to reduce statistical errors and to match the scan duration (e.g., 5 min) of particle measurements. A typical mass spectrum taken from ambient air is shown in Figure 2a.

[13] We note that our H_2SO_4-CIMS directly measures ambient gas phase H_2SO_4 (monomer) concentrations, as opposed to naturally formed neutral or charged H_2SO_4 clusters. Indirect calibration of H_2SO_4 can be made with OH radicals on the basis of the following reactions [*Eisele and Tanner*, 1991; *Tanner and Eisele*, 1995]:

$$OH + SO_2 \rightarrow HSO_3, \quad \text{(R2)}$$

$$HSO_3 + O_2 \rightarrow SO_3 + HO_2, \quad \text{(R3)}$$

$$SO_3 + H_2O \rightarrow H_2SO_4. \quad \text{(R4)}$$

We have made tests using this method and found that the measured $[H_2SO_4]$ by CIMS are in good agreement with the measured [OH] within the experimental uncertainties [*Benson et al.*, 2008; *Young et al.*, 2008], which also confirms that the H_2SO_4 monomers are detected. It is also possible that in the ion molecule reaction region, NO_3^- ions can make clusters, such as NO_3^-▪$(HNO_3)_m$, where m = 1, 2, 3… etc., and NO_3^-▪$(H_2O)_n$, and n = 1, 2, 3… etc. Laboratory measurements have showed that these clusters also react with H_2SO_4 to produce corresponding clusters [*Viggiano et al.*, 1997]:

$$NO_3^- \text{▪} (HNO_3)_m + H_2SO_4 \rightarrow HNO_3 + HSO_4^- \text{▪} (HNO_3)_m, \quad \text{(R5)}$$

$$NO_3^- \text{▪} (H_2O)_n + H_2SO_4 \rightarrow HNO_3(H_2O)_m + HSO_4^- \text{▪} (H_2O)_{n-m}. \quad \text{(R6)}$$

The reaction rates of reactions (R5) and (R6) are approximately 1.8×10^{-9} cm^{3}s^{-1}, in a similar range as that of reaction (R1) [*Viggiano et al.*, 1997]. In order to avoid this complexity, collision dissociation chamber (CDC) was used to dissociate these weakly bonded ion clusters via low-energy collisions with N_2 molecules.

2.2.3. NH_3-CIMS

[14] NH_3-CIMS is identical to the H_2SO_4-CIMS except for the ion-molecule reaction region. Whereas H_2SO_4-CIMS operates at atmospheric pressure with negative ion chemistry (reaction (R1)), NH_3-CIMS operates at low pressure (2670–3330 Pa) with the following positive chemical ionization (CIMS) reaction [*Huey*, 2007; *Nowak et al.*, 2007]:

$$(C_2H_5OH)_nH^+ + NH_3 \rightarrow NH_3(C_2H_5OH)_{n-m}H^+ + m(C_2H_5OH), \quad \text{(R7)}$$

where m is an integer less than or equal to n. Primary reagent ions seen in CIMS spectra, in the order of decreasing ion intensity, were protonated ethanol dimer $(C_2H_5OH)_2H^+$ (93 amu), trimer $(C_2H_5OH)_3H^+$, (139 amu) and monomer $(C_2H_5OH)H^+$ (47 amu). Primary product ions were $(C_2H_5OH)NH_4^+$ (64 amu), NH_4^+ (18 amu) and $(C_2H_5OH)_2NH_4^+$ (110 amu) (Figure 2b). Only the product ion signal at 64 amu was used for $[NH_3]$ calculations, since this was the most prominent ion peak (Figure 2c) and gave the best sensitivity. To account for the possible fluctuations in reagent ion signals which were caused by the fluctuation of pressure in the ion-molecule reaction region (<10%), we also monitored these primary reagent ions and normalized them when calculating $[NH_3]$.

[15] The sampling inlet was built on the basis of several configurations discussed by *Nowak et al.* [2006, 2007]. While for H_2SO_4 measurements the CIMS sensitivity is the key technical issue, for NH_3 measurements the critical issues are low background signals, reliable calibration (or instrument sensitivity) and fast time response. The NH_3-CIMS experimental setup is described in detail elsewhere (D. R. Benson et al., Chemical ionization mass spectrometer for ambient ammonia measurements, manuscript in preparation, 2010). Briefly, ambient air was drawn via a 1/4 inch PFA Teflon tube into a three-way valve that either allows ambient air to flow directly into the CIMS (ambient mode) or reroutes it through a scrubber that removes NH_3 from ambient air (background mode) and then to CIMS. The residence time is about 100 ms and 160 ms in the ambient and background mode, respectively. In order to determine the CIMS instrument sensitivity, calibration gases were added to the ambient gases and the difference in ion signal between the calibration and ambient mode was used for the sensitivity estimation. Care was taken to minimize the dead volume in the calibration system and at the optimum condition the time response was estimated to be <10 s. A computer program was used to automatically switch measurements between the background, ambient and calibration mode with a programmed sequence (Figure 2c).

[16] Ambient $[NH_3]$ were calculated from the differences in total product signals taken during the ambient and the consecutive background mode, further multiplied by the average CIMS sensitivity. For the example shown in Figure 2c

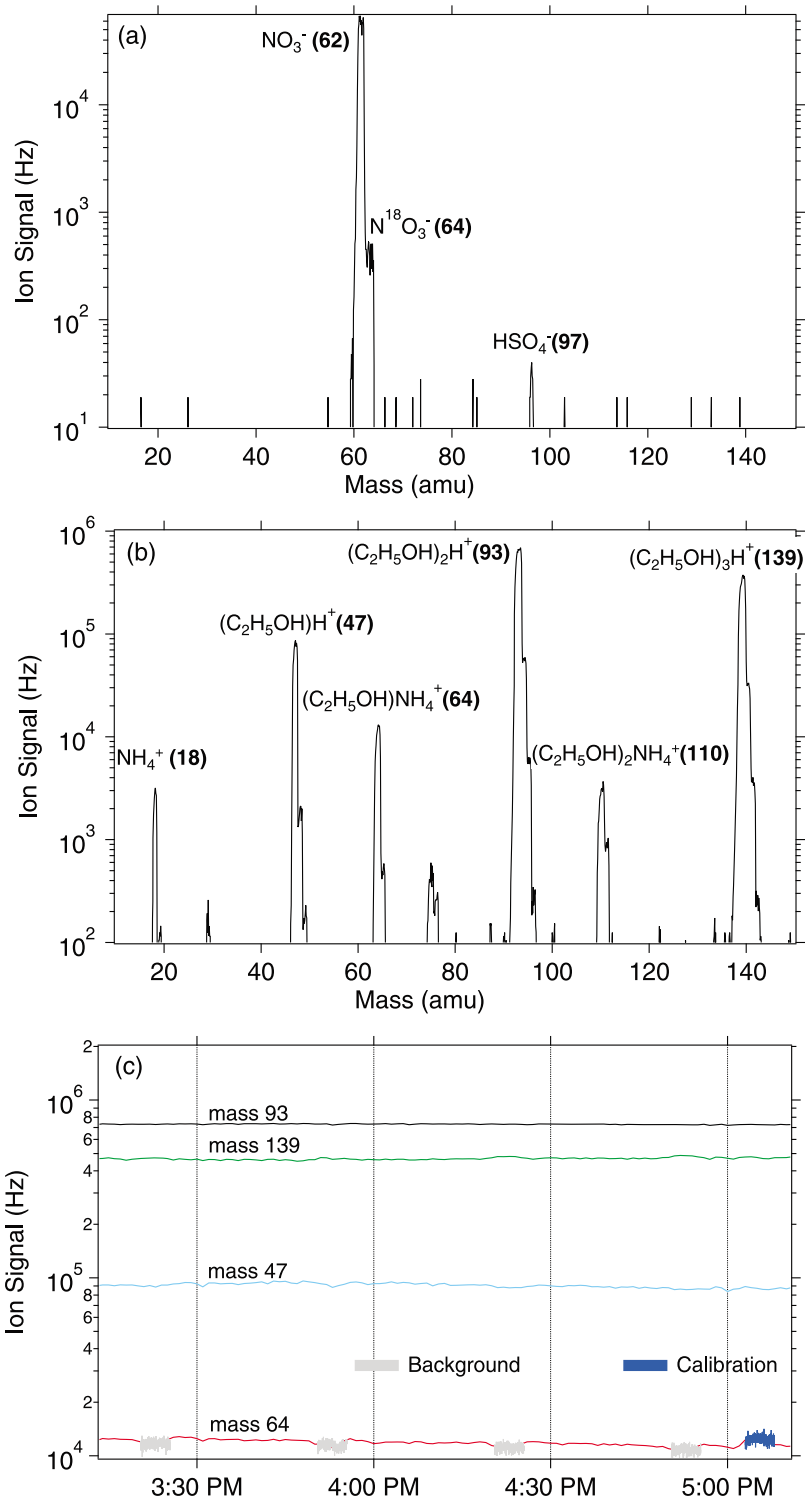

Figure 2. Typical CIMS mass spectra for (a) H_2SO_4 and (b) NH_3 detection. (c) An example of a typical sequence used for NH_3 background, ambient, and calibration measurements: included are the strongest NH_3 product ion signal (amu 64) and all three reagent ion signals (amu 93, 139, and 47; see section 2.2.3). The background (light gray) and calibration (blue) modes are indicated here, and the measurements made during other times correspond to the ambient mode.

(29 October 2009), the 64 amu signals during the calibration, ambient, and background mode were approximately 12,700, 11,500 and 10,500 Hz, respectively. Since 200 pptv of standard gas was used, the sensitivity was estimated to be 6 Hz/pptv. In this case, the background and ambient [NH_3] were estimated to be 1750 pptv and 170 pptv, respectively. Typically, the detection limit of NH_3-CIMS was ~60 pptv and the overall uncertainty associated with the instrument background and the sensitivity was 30 pptv ± 30% (D. R. Benson et al., manuscript in preparation, 2010).

2.2.4. Weather and Backward Trajectory Data

[17] We measured ambient relative humidity (RH) and temperature using a temperature/humidity sensor (Campbell Scientific CS215). The RH sensors were calibrated and are NIST and National Physical Laboratory (NPL) traceable, and had an accuracy of ±4% over RH from 0 to 100%. Weather data, including wind direction and speed, were also taken from the local weather station [41.15 N, 81.36 W] data archive website www.wunderground.com. Backward trajectory data were calculated with the PC version program of HYSPLIT (Draxler, R. R. and Rolph, G. D. HYSPLIT: Hybrid Single-Particle Lagrangian Integrated Trajectory Model, 2010, available at http://ready.arl.noaa.gov/HYSPLIT.php).

3. Data Analysis Methods

[18] Aerosol size distributions measured from a nano-DMA (TSI 3085) and a long-DMA (TSI 3081) were merged together into the size range from 3 to 1000 nm. The purpose of using two DMAs was to estimate the condensation sink from the complete aerosol size range. The nano- and long-DMA measurement data were not always identical and there were some differences, for example, 30% for the 3 May 2009 measurement (Figure 5) between the two measurements for the overlapping size range (e.g., 25–100 nm). Since we focused on the nanometer size particles, we took nano-DMA data for the size range from 3 to 102 nm. After this merging, particle number concentrations in various size ranges (e.g., particles in the size range from 3 to 25 nm, N_{3-25}, and from 3 to 1000 nm, N_{total}) were calculated.

[19] Classification of NPF events was made visually on the basis of the shape of aerosol size distributions in a manner similar to *Dal Maso et al.* [2005]. Events were characterized by a burst of N_{3-25}, followed by at least 2 h of persistent particle growth. Aerosol size data was then synchronized with [H_2SO_4], [NH_3], weather, and trajectory data. The measurement and meteorological data were averaged over a certain time period (e.g., 30 min typically) and used to calculate other key parameters, such as J (section 3.1), GR (sections 3.1 and 3.2), H_2SO_4 production rate (Q_{H2SO4}) (section 3.3), condensation sink (CS) (section 3.3), and time delay (Δt) between the [H_2SO_4] and N_{3-25} diurnal peaks (section 3.3).

3.1. Calculation of Particle Nucleation (J) and Growth Rates (GR) With PARGAN Model

[20] To calculate nucleation rates (J) and growth rates (GR) from ambient measurements of aerosol size distributions, we have used an inversion program, Particle Growth and Nucleation (PARGAN) [*Verheggen*, 2004; *Verheggen and Mozurkewich*, 2006]. This model has been described in detail elsewhere [*Verheggen*, 2004; *Verheggen and Mozurkewich*, 2006] and the PARGAN user interface is available at http://iacweb.ethz.ch/php/pargan/. Briefly, the input of the PARGAN model is the banana-shaped aerosol size distribution data, and the output is GR, on the basis of which J values are further derived (e.g., Figure 6a). PARGAN derives GR and J values from the measured aerosol size distributions with the inversion method, by assuming that consecutive measurements at the same site are representative of the history of the air mass. This assumption is not specific to PARGAN, as it also applies to other methods to derive GR from the measurements. The nucleation rates are calculated solely on the basis of the aerosol measurements, independent of any nucleation theories or parameterizations. In PARGAN, the particle GR is determined by nonlinear regression analysis of the General Dynamic Equation (GDE) [*Friedlander*, 2000] that best fits the measured change of aerosol size distributions over time. It does not provide a simulation of concentration time series, as forward modeling does; the observed size distributions are instead used as input for the model. Knowing the GR as a function of time enables the evaluation of the time of nucleation of measured particles of a certain size. J is then obtained by integrating the particle losses from the time of measurement to the time of nucleation. The program includes a full description of aerosol microphysical dynamics (condensation, coagulation, deposition, and dilution), of which several factors can act as fit parameters. Determination of GR_{PARGAN} via regression analysis provides more detailed information on the time evolution of GR than the common method of fitting a curve through the banana-shaped contour plot of consecutive size distributions or taking the time derivative of the modal diameter (GR_{MODAL}). On the other hand, GR_{PARGAN} is also sensitive to noise or variability in aerosol size measurements, as indicated by the nondistinctive banana-shaped size distributions resulted from air mixing.

3.2. Other Methods to Calculate Growth Rates (GR)

[21] In addition to GR_{PARGAN}, we have also used two additional methods to calculate GR, one from H_2SO_4 condensation (GR_{H2SO4}) and another from changes in the measured aerosol modal diameters over time (GR_{MODAL}). Comparisons of growth rates from these three different methods are discussed in section 5.1.

[22] The approach used to calculate GR_{H2SO4} was based on the assumption that all particle growth occurs by condensation of H_2SO_4 and H_2O in the kinetic condensation regime [*Seinfeld and Pandis*, 2006]. So GR_{H2SO4} (nm h^{-1}) can be expressed as

$$GR_{H2SO4} = \frac{3600 \cdot 10^9 \cdot M_s c^{-\alpha} \alpha \left([H_2SO_4] - [H_2SO_4]_{eq} \right) W_R}{(2\rho/10^3) \cdot 6.022 \cdot 10^{23}}, \quad (2)$$

$$c^{-\alpha} = \left(\frac{8 \cdot 10^3 \cdot RT}{\pi M_s} \right)^{1/2}, \quad (3)$$

where M_s is the molecular weight of H_2SO_4 (98 g mol^{-1}), c is the mean speed of H_2SO_4 vapor (m s^{-1}), α is the mass transfer accommodation coefficient (unity is used here), $[H_2SO_4]_{eq}$ (molecules cm^{-3}) is the equilibrium concentra-

tion of H_2SO_4 (usually $[H_2SO_4] \gg [H_2SO_4]_{eq}$), W_R is the ratio of the wet H_2SO_4 particle diameter at a certain RH to that of the dry H_2SO_4 diameter (e.g., W_R = 1.3 at RH = 20%), ρ is the particle density (1,400 kg m^{-3}), and R is universal gas constant (8.314 Joules mol^{-1} K^{-1}), and T is temperature (K). The same or similar method has been used by atmospheric observations [*Paasonen et al.*, 2009; *Sihto et al.*, 2006; *Stolzenberg et al.*, 2005; *Verheggen and Mozurkewich*, 2002; *Weber et al.*, 1997, 1998; *Young et al.*, 2008], modeling simulations [*Kerminen and Wexler*, 1996; *Verheggen and Mozurkewich*, 2006], and laboratory kinetic studies [*Young et al.*, 2008]. While the water effects on particle growth are taken into account in equation (2) since W_R is dependent on RH, growth by ammonia is not considered here. Recent studies have showed that ammonia does not effectively contribute to aerosol growth [*Zhang et al.*, 2009], and the condensation of $(NH_4)_2SO_4$ can be in fact similar to that of H_2SO_4 [*Weber et al.*, 1998].

[23] Another approach was also used to directly calculate GR_{MODAL} from the changes in the measured particle mean diameters (D_p) over the lapse time of the nucleation event [*Paasonen et al.*, 2009; *Sihto et al.*, 2006; *Stolzenberg et al.*, 2005]. GR_{MODAL} obtained by this method reflects the overall effect of various aerosol dynamic processes (i.e., condensation, coagulation, and dilution loss) occurring in that time window. GR_{MODAL} is sensitive to signal, whereas GR_{PARGAN} is sensitive to both signal and noise.

3.3. Estimation of Condensation Sink (*CS*), H_2SO_4 Production Rate (Q_{H2SO4}), and Time Delay (Δt) Between H_2SO_4 and NPF

[24] Preexisting particles in the atmosphere are the sink of aerosol nucleation, as they provide the surface area for condensation of aerosol precursors and small particles can also coagulate with these particles to be scavenged. The condensation sink (*CS*), defined as the rate at which condensable vapors condense on existing particles, was calculated on the basis of the following equations [*Kulmala et al.*, 2001a]:

$$CS = 2\pi D \cdot 10^{-7} \int_0^{\infty} d_p \beta_m(d_p) n(d_p) dd_p = 2\pi D \cdot 10^{-7} \sum_i \beta_{m_i} d_{p_i} N_i, \quad (4)$$

$$\beta_m = \frac{1 + Kn}{1 + 0.337Kn + \frac{4Kn}{3\alpha} + \frac{4Kn^2}{3\alpha}}, \quad (5)$$

$$Kn = \frac{2\lambda_v}{d_p}, \quad (6)$$

where d_p is particle diameter (nm), β_m is transition correctional factor (dimensionless) [*Fuchs and Sutugin*, 1971], *Kn* is the Knudsen number (dimensionless), D is diffusion coefficient (D = 0.104 cm^2 s^{-1} under our typical RH [*Hanson and Eisele*, 2000]), λ_v is the mean free path of the vapor molecules (123 nm), N_i is particle number concentration in size bin i, α is the mass accommodation (taken to be unity), and $n(d_p)$ is particle size distribution function.

[25] The production rate of H_2SO_4 (Q_{H2SO4}) is defined as $k[SO_2][OH]$ based on reaction (R2). However, since we did not have measurements of $[SO_2]$ and [OH], we reversely estimated Q_{H2SO4}, using the measured $[H_2SO_4]$ and *CS*, by assuming steady state for $[H_2SO_4]$. In practice, during the nucleation process, $[H_2SO_4]$ can be expressed as a function of time:

$$\frac{d[H_2SO_4]}{dt} = Q_{H2SO4} - CS[H_2SO_4]. \quad (7)$$

If we assume steady state for $[H_2SO_4]$, as H_2SO_4 molecules rapidly condense on existing particles and so their H_2SO_4 lifetimes are sufficiently short, then

$$\frac{d[H_2SO_4]}{dt} = 0. \quad (8)$$

From equations (7) and (8), we obtain the following relationship:

$$Q_{H2SO4} - CS[H_2SO_4]. \quad (9)$$

It is also common that atmospheric $[H_2SO_4]$ and new particles (e.g., N_{3-25}) have different time dependencies during NPF events and therefore, when we investigate the relationship of J to the measured $[H_2SO_4]$, it is also necessary to know the time delay (Δt), which is the difference in timing between the peaks of $[H_2SO_4]$ and N_{3-25}. We adopted the fitting method similar to the one used by *Paasonen et al.* [2009], *Riipinen et al.* [2007], and *Sihto et al.* [2006] to determine the time delay (Δt). The time shift is referred to as the time difference in diurnal trend of aerosol precursors and particle number concentration and is also interpreted as the duration of particle formation, during which critical clusters grow to measurable particle sizes. This Δt was taken into account for performing $J = C[H_2SO_4]^P$ fitting, where J is the nucleation rate, C is preexponential factor and P is exponent; P is considered as the number of H_2SO_4 molecules in the critical cluster (section 4.4).

4. Results

4.1. Characteristics and Frequency of NPF in Kent, Ohio

[26] From August 2008 to November 2009, there were a total of 83 days of simultaneous observations of particles together with H_2SO_4 and/or NH_3 (Table 2). Among, there were 27 days in which all three measurements were made together. Another 56 days also involved the particle measurements with either H_2SO_4 or NH_3 (42 days with H_2SO_4 only and 14 days with NH_3 only). In total, there were 32 NPF days, 27 non-NPF days and 24 undefined days. During the NPF events, the median N_{3-25} ranged from 200 to 10,300 cm^{-3}. The frequency of NPF during this simultaneous measurement period was 66% in spring, 47% in fall, 23% in summer and 22% in winter. In general, this trend measured from August 2008 to November 2009 was in agreement with our long-term particle measurements made from January 2006 to December 2009, which showed the higher frequency during the spring (45%) and fall (31%) and lower frequency during the summer (17%) and winter (6%) (Table 2) (L.-H. Young et al., manuscript in preparation,

Table 2. Summary of Seasonal Measurements of [H_2SO_4], [NH_3], Condensation Sink (*CS*), and Size-Resolved Particle Number Concentrations Including N_{total} and $N_{3–25}$[a]

	Winter (9 Days): 22 Dec 2008 to 1 Jan 2009	Spring (18 Days): 23 Apr to 10 May 2009	Summer (26 Days)		Fall (30 Days)	
			23–25 Aug 2008	9–31 Aug 2009	1–4 Sep 2008	29 Oct to 1 Dec 2009
Daily N_{total} range (10^3 cm^{-3})	1.5–5.7	4.9–14.4	6.1–19.7	1.2–10.4	6.1–10	0.8–12.0
Daily N_{total} median (10^3 cm^{-3})	3.6	8.3	8.8	5.5	9	2.5
Daily $N_{3–25}$ range (10^3 cm^{-3})	0.3–1.3	1.1–6.8	0.7–10.3	0.2–2.0	0.8–1.2	0.2–7.8
Daily $N_{3–25}$ median (10^3 cm^{-3})	0.8	2.1	0.9	0.5	1	0.6
Daily *CS* range (10^{-3} s^{-1})	2–8	6–21	8.5–28.7	1.7–38.5	15–27	0.6–11.4
Daily *CS* median (10^{-3} s^{-1})	4	11	15.9	12.9	23.5	3.6
Daily noontime peak range [H_2SO_4] (10^6 cm^{-3})	0.3–1.4	2.2–9.8	1.3–15.7	1.1–45.7	0.9–1.3	<0.2–3.5
Daily noontime peak median [H_2SO_4] (10^6 cm^{-3})	0.6	5.2	2.9	2.9	0.5	0.5
Daily [NH_3] range (pptv)	<50–250	<50–430	NA	NA	NA	<50–300
Daily [NH_3] median (pptv)	60	200	NA	NA	NA	150
NPF days/measurement days (% frequency)	2/9 (22%)	12/18 (66%)	6/26 (23%)	6/26 (23%)	14/30 (47%)	14/30 (47%)
Overall frequency (2006–2009) (% frequency)[b]	11/177 (6%)	86/192 (45%)	29/167 (17%)	29/167 (17%)	44/140 (31%)	44/140 (31%)

[a][NH_3] and [H_2SO_4] were measured by CIMS. The CIMS NH_3 detection limit is 60 pptv, while the CIMS H_2SO_4 detection limit is ~2×10^5 cm^{-3}.
[b]More detailed results for long-term trend of new particle formation observed in Kent are given by L.-H. Young et al. (manuscript in preparation, 2010).

2010). These NPF frequencies observed in Kent were also consistent with the observations made in other locations, such as Pittsburgh [*Stanier et al.*, 2004] and Finland [*Kulmala et al.*, 2001b].

[27] The distinction between NPF and non-NPF was clear from the plot of particle size distributions (Figures 3a and 3b), as the NPF events were characterized with a characteristic banana shape (e.g., 4 October 2008 in Figure 3a, as opposed to 27 December 2008 in Figure 3b). The NPF and non-NPF events were also distinguishable by examining particle number concentrations as a function of particle diameter (D_p). For example, as shown in Figure 3c, on 4 October 2008 (NPF) there were not many particles between 0600 and 0900 LT, but shortly thereafter (1100–1400 LT) the size distributions started to change dramatically with the appearance of large concentration of $N_{3–25}$, indicating that nucleation was taking place. The size distribution during this period (1100–1400 LT) had another smaller mode at ~60 nm. The nucleation burst was followed by the sustained growth reaching ~60 nm between 1600 and 1900 LT. In contrast, on 27 December 2008 (non-NPF), the number concentrations and size distributions were nearly constant (except for size range 40–80 nm where there were occasional low concentrations of particles) during 0600–0900, 1100–1400, and 1600–1900 LT.

4.2. NPF in Relation to Seasonal and Diurnal Variation of H_2SO_4 and NH_3

[28] During the NPF days (marked by brown bars on top of Figures 4a–4d), $N_{3–25}$ usually increased between 0900 and 1400 local time and showed a clear diurnal pattern. In general, condensation sink (*CS*) appeared to be decreasing (suggestive of air mixing) at the onset of nucleation, reaching a minimum point during the peak of $N_{3–25}$. [H_2SO_4] also had a distinct diurnal pattern and often preceded $N_{3–25}$, with the highest concentrations during day time (10^6–10^7 cm^{-3}) and the lowest during nighttime (lower 10^5 cm^{-3}). The rapid increase in [H_2SO_4] after sunrise followed by a decrease after sunset indicates that the H_2SO_4 formation involves photochemical processes. The median noontime [H_2SO_4] was higher in the spring (5.2×10^6 cm^{-3}) and summer (2.9×10^6 cm^{-3}) and lower in the winter (0.6×10^6 cm^{-3}) and fall (0.5×10^6 cm^{-3}). This seasonal trend of [H_2SO_4] also coincided with the NPF frequency. The threshold [H_2SO_4] for NPF in Kent was ~1×10^6 cm^{-3} (Figure 7c). All the NPF days had higher [H_2SO_4] in general, but it was also true that the days with high [H_2SO_4] were not necessary the NPF days. For example, between 14 August 2009 and 25 August 2009, the noontime [H_2SO_4] ranged from 10^6–10^7 cm^{-3}, but there was no NPF observed. These non-NPF days with the high [H_2SO_4] were mostly frequently found during the summer (23 days); but there was no such a case in spring. Unlike [H_2SO_4], the measured [NH_3] showed no clear diurnal pattern, although there were some rapid hourly variations. The daily median mixing ratios were slightly higher in spring (300 pptv) and fall (250 pptv) than in winter (70 pptv). While the relationship between the diurnal patterns of H_2SO_4 and $N_{3–25}$ was clear during the NPF events, this was not the case for NH_3.

4.3. Case Study of Strong NPF: 3 May 2009

[29] We have chosen 3 May 2009 (Figures 5 and 6) to represent a typical NPF day in Kent, as the NPF frequency was highest during the spring. On this day, for the period shortly before 1200 LT when nucleation took place, the RH ranged from 28 to 33% with the temperature ranging from 17 to 19°C (Figure 5a). The median values of N_{total}, $N_{3–25}$ and *CS* were 10,000 cm^{-3}, 2000 cm^{-3}, and 0.011 s^{-1}, respectively. The particle size distribution displayed a distinctive banana shape (Figure 5b) and the burst in $N_{3–25}$ took place close to 1200 LT coinciding with a sharp decrease in *CS* (Figure 5c). Figure 5c also presents results of comparisons of $N_{3–25}$ measured by the water- and butanol-CPC. As shown by [*Young et al.*, 2008], these ratios can provide indirect information on the chemical composition of aerosol particles, with respect to the relative amounts of H_2SO_4 versus organic components. Generally, the water-CPC showed higher $N_{3–25}$ than the butanol-CPC by a factor of

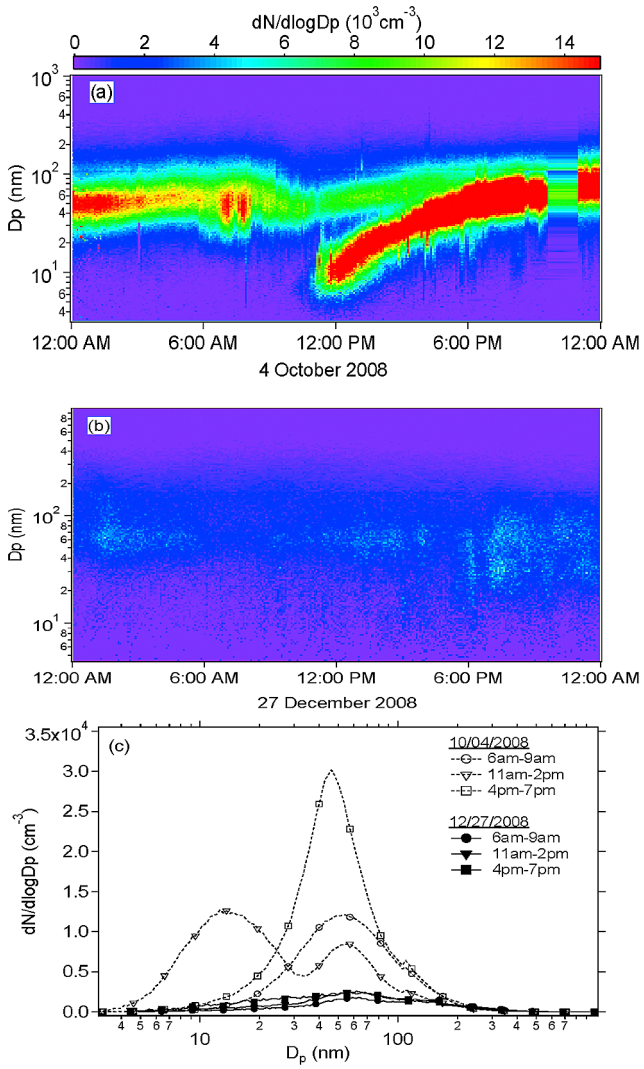

Figure 3. Aerosol size distributions for (a) a typical NPF (4 October 2008) and (b) non-NPF (27 December 2008) events observed in Kent, Ohio. (c) The measured particle number concentrations as a function of particle diameter (D_p) averaged over different time periods for these two days. Local times were used in the present study.

~2. This ratio was fairly constant throughout the day except for the major change in the ratio seen between ~1000 and 1200 LT when $N_{3–25}$ concentrations started to increase dramatically to ~25. This implies that the freshly nucleated particles initially contained more H_2SO_4 (ratio ~25) and the composition likely changed during particle growth (ratio ~2). H_2SO_4 had a clear diurnal variation with the median noon time peak concentration of 2.2×10^6 cm^{-3}. On the other hand, [NH_3] was in the range from 200 to 400 pptv and had no diurnal variation, although there were rapid hourly variations. (Figure 5d).

[30] Figure 6a shows the calculation results from PARGAN using the observed aerosol size distribution, where *GR* and *J* are plotted as a function of local time. These values of GR_{PARGAN} and J_{PARGAN} were calculated between 1200 and 1250 LT; other times where GR_{PARGAN} were negative owing to inhomogeneous air masses are not shown here. The median GR_{PARGAN} and J_{PARGAN} values were 7.3 nm h^{-1} and 4.2 cm^{-3}s^{-1}, respectively. J_{PARGAN} above was used to investigate its connection with [H_2SO_4] by performing Log J_{PARGAN} versus Log [H_2SO_4] fitting (Figure 6b). The results of this fitting show $J_{PARGAN} = C[H_2SO_4]^P$, with P = 1.9 and Log C = −11.6. The median GR_{PARGAN} (7.3 nm h^{-1}) was comparable to GR_{MODAL} (6.8 nm h^{-1}). On the other hand, the median GR_{H2SO4} calculated by considering H_2SO_4 as the only condensable species was a factor of 34 lower than GR_{MODAL} (Figure 6c). No relationship between NH_3 and NPF was also discerned. These results imply that other species, most likely organic compounds, also played a role in the growth of nucleated particles [*Smith et al.*, 2010; *Zhang et al.*, 2009]. This was a calm day (Figure 6d) and the observed NPF were favored by clear skies (hence higher H_2SO_4) and lower *CS*. Clean air from the free troposphere may have contributed to the lower *CS* as shown by hourly back trajectories (Figure 6e).

4.4. *J* and *GR* Correlation With [H_2SO_4] and [NH_3]

[31] There were a total of 11 NPF days (5 days in spring, 4 days in summer, and 2 days in fall), in which we were able to calculate meaningful values of *GR* and *J* with PARGAN (Figure 7a and Table 3). These were days that had the distinctive banana shape in measured aerosol size distributions.

[32] The time delay (Δt) between the [H_2SO_4] and $N_{3–25}$ hourly peaks varied from Δt = 0 (24 August 2008) to Δt = 2.25 h (25 August 2009) (Table 3). The Δt values were not correlated with [H_2SO_4], which also imply that H_2SO_4 is not the only condensing species for aerosol nucleation and growth. Results of Log J_{PARGAN} versus Log [H_2SO_4] show that the measured J_{PARGAN} and [H_2SO_4] were positively correlated; J_{PARGAN} were dependent to [H_2SO_4] with the power of 0.6 to 2.3 and the Log C of −15.7 to −2.8 (Figure 7a and Table 3). Figure 7b shows a composite fit of time-shifted Log $N_{3–25}$ versus Log [H_2SO_4] for the NPF days. There was an almost linear dependence between Log $N_{3–25}$ and Log [H_2SO_4] (slope = 0.6). In the case of NH_3, Log J_{PARGAN} did not reveal any correlation with Log [NH_3], as [NH_3] did not vary much during the course of the day (Figure 7c).

[33] Although the number of NPF days in which we were able to calculate *J* from PARGAN were a few, from these limited data we can conclude that the median J_{PARGAN} appeared to be higher during spring (8.8 cm^{-3} s^{-1}) followed by summer (4.1 cm^{-3} s^{-1}) and lowest in late fall (0.8 cm^{-3} s^{-1}) (Table 3). Also, GR_{MODAL} and GR_{PARGAN} were higher in summer and lower during spring and winter (Figure 7d). GR_{MODAL} were 6.3–83 times higher than GR_{H2SO4} (Table 3 and Figure 7d).

[34] From the observation results taken in Kent, it seems that different factors may have contributed to the low NPF frequency seen during the summer and winter. The low NPF frequency, as well as low nucleation rates and growth rates, observed during the winter were mostly likely due to low [H_2SO_4], usually lower than the threshold [H_2SO_4] for NPF (~1×10^6 cm^{-3}). In summer, high temperatures and strong sunlight produce VOCs, and it is possible that some of these VOCs may have suppressed OH concentrations and thus nucleation [*Kiendler-Scharr et al.*, 2009]. On the other hand, the oxidation products of these organic species may

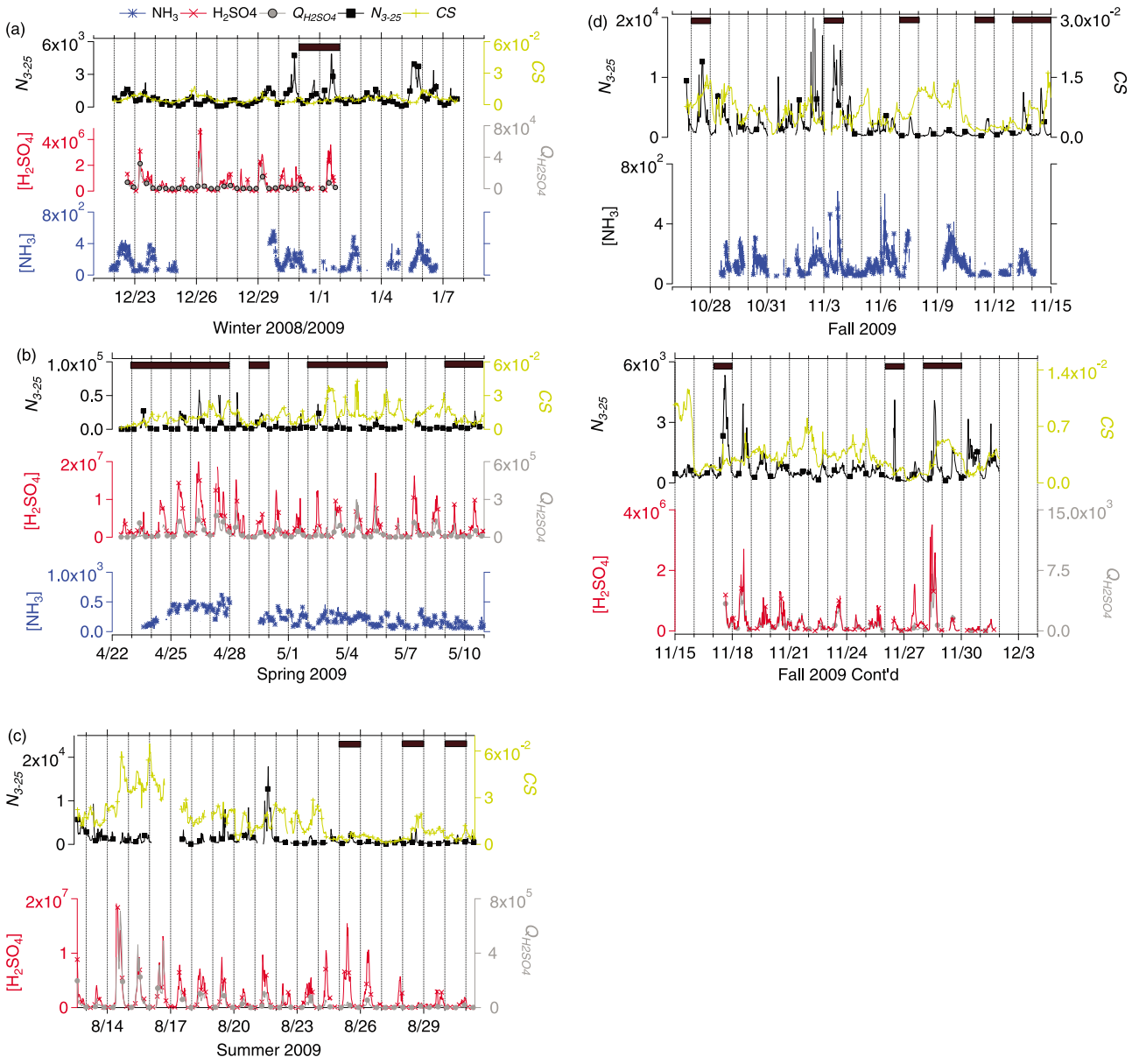

Figure 4. The measured $N_{3–25}$ (cm^{-3}) (black squares), $[H_2SO_4]$ (cm^{-3}) (red crosses), and $[NH_3]$ (parts per trillion by volume) (blue asterisks), the derived condensation sink CS (s^{-1}) (orange pluses), and sulfuric acid production rate Q_{H2SO4} (cm^{-3} s^{-1}) (gray circles) in (a) winter, (b) spring, (c) summer, and (d) fall. For the summer data, we had measurements both in 2008 and in 2009 (Table 2), but the 2008 data are not shown here since there were only 3 days of measurements. The same applies to the fall data: the 2008 data are not shown here. The dark brown horizontal bars on top of the plots indicate days that had NPF.

also be likely responsible for the higher growth rates seen during the summer.

5. Discussion

5.1. Evaluation of GR_{PARGAN} and J_{PARGAN}

[35] An important issue related to NPF studies is how nucleation rates (J) and growth rates (GR) are derived from ambient particle size and number concentrations. Currently available commercial particle instruments usually detect particle sizes starting from 3 nm, above 1–1.5 nm, which is considered as the critical cluster size [*Kulmala and Kerminen*, 2008]. J values calculated using the measured aerosol number concentrations (thus, apparent nucleation rate) do not take into account condensation and coagulation processes, which occur before critical clusters grow to measurable size (>3 nm). Therefore, indirect methods have been employed to estimate J of 1 nm cluster (J_1) from apparent nucleation rates (for example, J_3 which is the nucleation rate derived from particle concentrations in the size range >3 nm). The most commonly used method is based on the time shift (or time delay, Δt) by using the measured aerosol size distribution and by taking into account self-coagulation of small particles and scavenging due to coagulation with

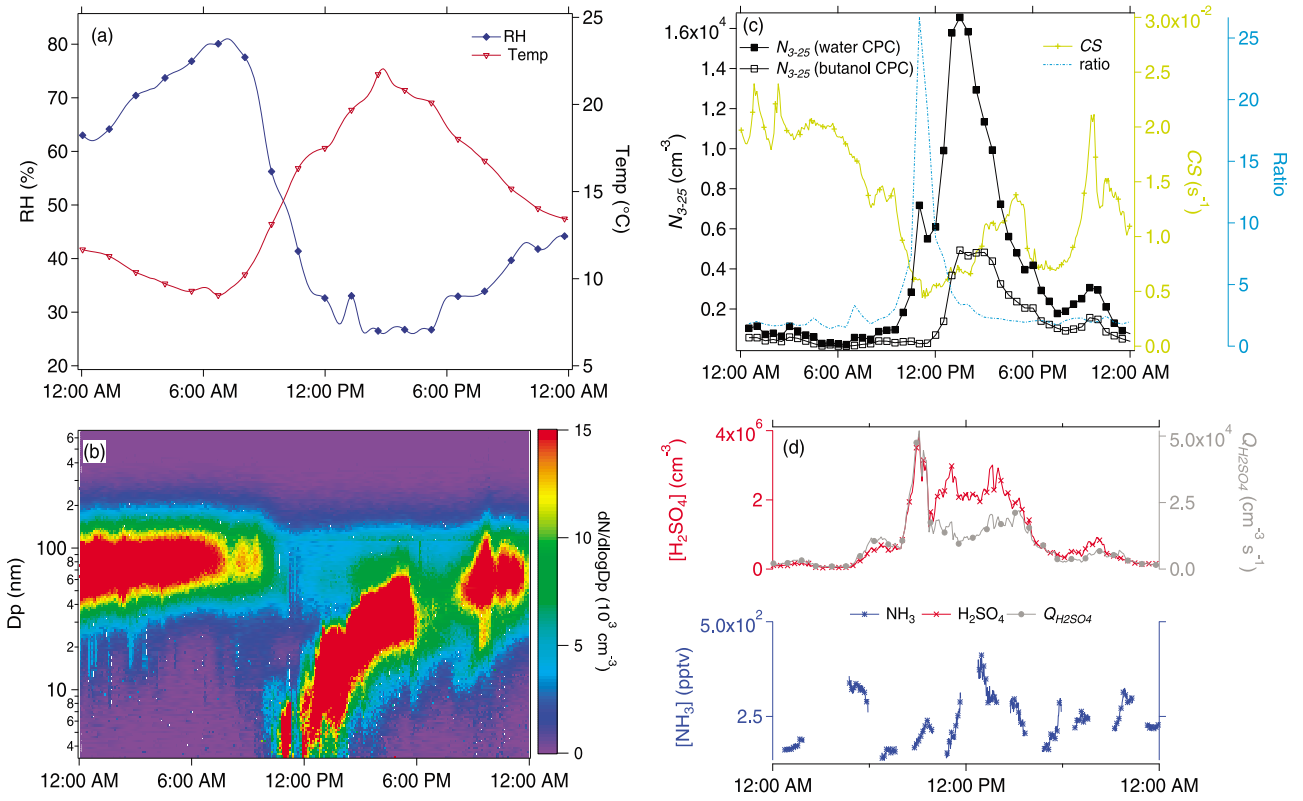

Figure 5. The measured and derived parameters for a case study of an NPF event in Kent on 3 May 2009. (a) Temperature (red triangles) and relative humidity (RH, blue squares), (b) particle size distribution, (c) $N_{3–25}$ measured by the water-CPC (solid squares) and butanol-CPC (open squares), the ratio of $N_{3–25}$ measured with the water-CPC to butanol-CPC (blue dashed line), and *CS* (condensation sink) (orange pluses), and (d) [H_2SO_4] (red crosses), [NH_3] (blue asterisks), and Q_{H2SO4} (H_2SO_4 production rate) (gray circles).

large particles [*Dal Maso et al.*, 2005; *Fiedler et al.*, 2005; *Kerminen and Wexler*, 1996; *Kuang et al.*, 2008; *Kulmala et al.*, 2004; *McMurry et al.*, 2005; *Paasonen et al.*, 2009; *Riipinen et al.*, 2007; *Sihto et al.*, 2006; *Stolzenberg et al.*, 2005; *Weber et al.*, 1996]. In practice, H_2SO_4 is considered as the aerosol precursor for this kind of time shift calculations, so by default this method also assumes that H_2SO_4 is the only condensable species for aerosol formation. GR calculated using time delay is highly dependent on how it is calculated and may vary substantially [*Sihto et al.*, 2009]. For this reason, we did not use time delay to calculate *GR*, and instead used Δt only for correlation analysis between *J* and [H_2SO_4].

[36] In this study, we employed the independent inversion model Particle Growth and Nucleation (PARGAN) [*Verheggen and Mozurkewich*, 2006] to determine particle nucleation (J_{PARGAN}) and growth rates (GR_{PARGAN}) by taking into account aerosol growth and loss by coagulation, solely based on the measured aerosol size distributions without using the time shift (Δt) or aerosol precursor concentrations (as described also in section 3.1). PARGAN has been used for nucleation rate measurements in smog chamber studies [*Metzger et al.*, 2010; *Verheggen and Mozurkewich*, 2006]. Since GR_{MODAL} and GR_{PARGAN} are both determined from particle size distributions, we expect their values to be comparable. This is an important point as J_{PARGAN} is derived from GR_{PARGAN}. Of the 11 days where we obtained GR_{PARGAN}, the majority GR_{PARGAN} were within 70% of GR_{MODAL}. The uncertainties in the derived GR_{PARGAN} were about 28% overall. The main difference was due to the high sensitivity of PARGAN to the input data; the sensitivity accounts for both the signal and the noise (e.g., Figure 6a).

[37] The fact that GR_{PARGAN} values are comparable to GR_{MODAL} (Table 3 and Figure 7d) and that the GR_{MODAL} to GR_{H2SO4} ratio was similar to that obtained in other clean environments (Table 1) provides validity to the calculated GR_{PARGAN} and J_{PARGAN} values. Values of J_{PARGAN} obtained in this study were in the range of 0.4–12.9 (cm^{-3} s^{-1}) (Table 3). Our Kent observations in terms of [H_2SO_4], *J* and *GR* were also very similar to those measured in Boulder, Colorado [*Kuang et al.*, 2008] (Table 1), both relatively small-size Northern American towns, despite the independent methods employed in the computation of *J*. In addition, our J_{PARGAN} values were also similar to other independent observations made in the clean boreal forest environment [e.g., *Kulmala et al.*, 2001b, 2006].

[38] Another important parameter related to aerosol formation is the ratio of GR_{MODAL} over GR_{H2SO4}, as this value is indicative of how much H_2SO_4 has contributed to aerosol growth. Generally, GR_{MODAL} was ~6.3–83 times higher than GR_{H2SO4} (see GR_{MODAL} to GR_{H2SO4} ratio in Table 3), implying that H_2SO_4 alone cannot explain the measured aerosol growth rates and other condensable species are also

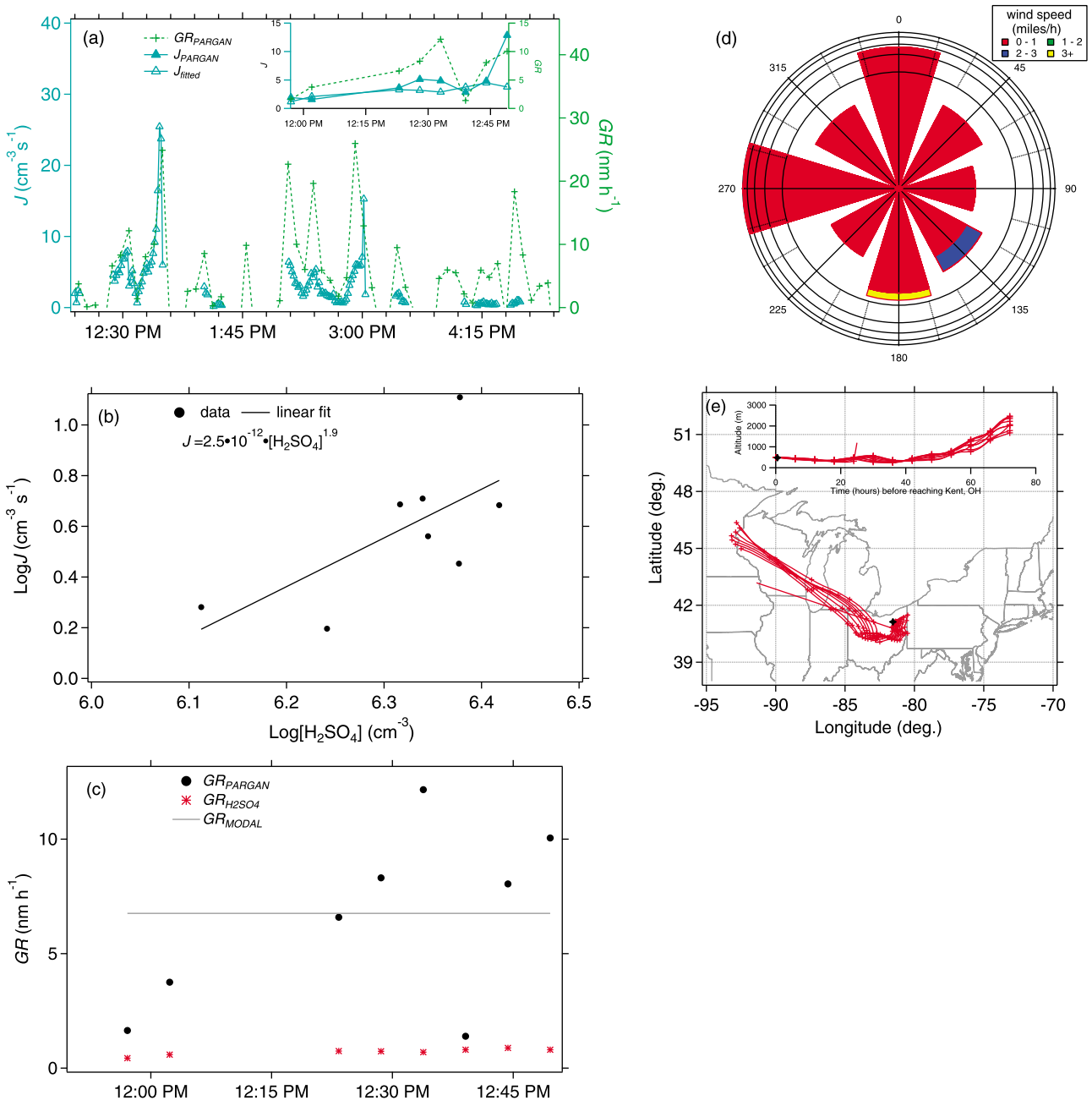

Figure 6. (a) Plot of GR_{PARGAN} (green pluses) and J_{PARGAN} (blue open triangles) as a function of local time on 3 May 2009. Shown in the inset are the averaged GR_{PARGAN} (green pluses) and J_{PARGAN} (blue open triangles) for the same period. J_{fitted} (blue solid triangles) was obtained from the Log J_{PARGAN} versus Log [H_2SO_4] fitting shown in Figure 6b. (b) Log J_{PARGAN} versus Log [H_2SO_4]. The same data used in Figure 6a were used here. The black solid line indicates linear fitting of the data. (c) The GR values obtained with three different methods: GR_{PARGAN} (black circles), GR_{MODAL} (gray line) and GR_{H2SO4} (red asterisks) (see sections 3.1 and 3.2). (d) A rose plot showing wind speed and direction on 3 May 2009. Different wind speeds are shown in different colors. (e) The NOAA Hybrid Single-Particle Lagrangian Integrated Trajectory (HYSPLIT) model 3-day back trajectories, for each hour of 3 May 2009. The inset shows the altitude profile of the air mass for each of these 24 trajectories as a function of time prior to reaching Kent.

required for aerosol formation. These results are also in good agreement with other simultaneous measurements of aerosol sizes and aerosol precursors, for example, at Idaho Hill, Colorado where the ratio of GR_{MODAL} versus GR_{H2SO4} was 5–10 [*Weber et al.*, 1997] and at Macquarie Island, Australia where this ratio was 4–17 [*Weber et al.*, 1998] (Table 1). These common findings also suggest that these additional "yet-unknown" ternary species must be not

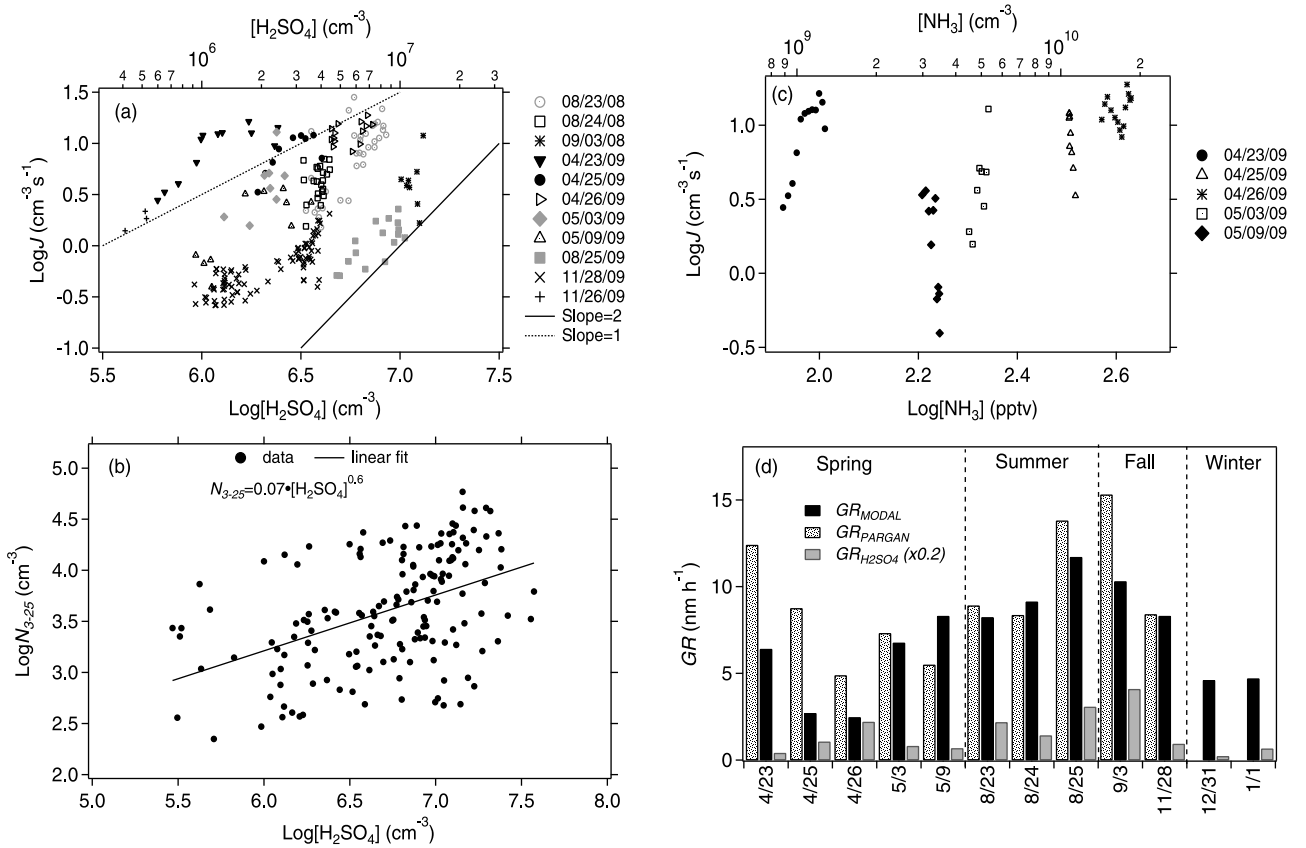

Figure 7. (a) Plot of Log J_{PARGAN} versus Log [H_2SO_4] for all the days that had the distinctive banana shape and [H_2SO_4]. The same data are also shown in Table 3 and Figure 7c. (b) Log $N_{3–25}$ versus Log [H_2SO_4] for the NPF days. The solid line indicates linear fitting of the data. (c) J_{PARGAN} versus Log [NH_3] for all the days that had the distinctive banana shape and [NH_3]. (d) Seasonal variation of *GR* obtained with three different methods: GR_{PARGAN} (stippled), GR_{MODAL} (black), and GR_{H2SO4} (gray) (see sections 3.1 and 3.2).

unique to the location and should exist in different atmospheric conditions.

5.2. H_2SO_4 Effects on Nucleation

[39] Most previous NPF studies have shown that J is proportional to the first or second power of [H_2SO_4]; that is, $J = C[H_2SO_4]^P$, where $P = 1$ or 2, and C is a preexponential factor [*Kuang et al.*, 2008; *McMurry et al.*, 2005; *Riipinen et al.*, 2007; *Sihto et al.*, 2006] (Table 1). These P value can also be interpreted as the number of H_2SO_4 molecules in the critical clusters on the basis of the classical nucleation theory [*Kashchiev*, 1982; *McGraw and Zhang*, 2008], under the assumption that nucleation takes place in a steady state condition [*McGraw and Zhang*, 2008]. However, C values were found to vary dramatically, over several orders of magnitude, at different locations and measurement periods, depending on unknown chemical and physical conditions. On the basis of this atmospherically observed relationship of $J = C[H_2SO_4]^P$, two empirical nucleation mechanisms have been proposed. For the case of $P = 1$, the activation mechanism assumes that nucleation takes place after activation of clusters containing one H_2SO_4 molecule, with the subsequent growth involving other condensable species [*Kulmala et al.*, 2006]. For the case of $P = 2$, the kinetics theory assumes that thermodynamically stable clusters are formed through collision of two H_2SO_4 molecules [*McMurry and Friedlander*, 1979]. While these theories can successfully explain the relationship between J and [H_2SO_4] found from atmospheric observations, these theories cannot reversely predict the nucleation rates solely from [H_2SO_4], because these unknown C values are difficult to characterize, and cannot be generalized, for different atmospheric conditions, suggesting that possibly the dominant nucleation mechanism(s) may vary with location and time.

[40] In Kent, NPF was almost always preceded by an increase in [H_2SO_4] on a daily basis, with time delay (Δt = 0–2.25 h) between the [H_2SO_4] and $N_{3–25}$ peaks, an indication that H_2SO_4 is an important nucleation precursor. There was no correlation between Δt and [H_2SO_4], implying that other condensable species, besides sulfuric acid, also play a role in aerosol growth from 1 to 3 nm size range. Our Δt values also agree with those found from other observations made in remote environments [*Marti et al.*, 1997; *Weber et al.*, 1996]. Also, the connection between J and [H_2SO_4] is similar to other ambient observations [*Fiedler et al.*, 2005; *Kulmala et al.*, 2006; *Weber et al.*, 1997] which found the power $P = 1–2$. On the other hand, recent laboratory experiments showed that at atmospheric pressure, 288 K and 10–55% RH, the threshold [H_2SO_4] needed for unit J value is in the range of 10^8–10^9 cm^{-3} and

Table 3. Summary of Conditions Including *GR* and the Log *J* Versus Log [H_2SO_4] Fitting Parameters During Nucleation Events in Which There Was a Distinctive Banana Shape to Allow *GR* and *J* Calculations With PARGAN[a]

Date	RH (%)	Temperature (°C)	Δt (min)	Range (Median)					*GR* (nm h^{-1})				J_{PARGAN} (cm^{-3} s^{-1})	*P*	Log *C*	*R*
				N_{3-25} (10^4 cm^{-3})	N_{total} (10^4 cm^{-3})	*CS* (10^{-3} s^{-1})	[H_2SO_4] (10^6 cm^{-3})	[NH_3] (pptv)	GR_{MODAL}	GR_{H2SO4}	GR_{PARGAN}	$\frac{GR_{MODAL}}{GR_{H2SO4}}$				
23 Apr 2009	47–38	11–14	75	0.1–1.0 (0.3)	0.3–2.5 (1.0)	4–11 (6)	0.7–2.4 (1.1)	100–111 (110)	6.4	0.1	12.4	64	11.5	1.0	−5.4	0.7
25 Apr 2009	47–45	21–23	105	0.1–3.2 (1.4)	0.2–3.3 (1.8)	6–12 (9)	2.0–4.1 (2.8)	420–430 (420)	2.7	0.2	8.8	13.5	8.8	1.3	−7.2	0.7
26 Apr 2009	39–37	23–25	85	0.1–6.3 (1.1)	0.4–6.6 (1.5)	9–14 (12)	4.–7.2 (5.2)	380–390 (380)	2.5	0.4	4.9	6.3	12.9	0.6	−2.8	0.5
3 May 2009	33–28	17–19	119	0.0–0.6 (0.2)	0.3–1.9 (1.0)	9–17 (11)	1.3–2.6 (2.2)	240–260 (250)	6.8	0.2	7.3	34	4.2	1.9	−11.6	0.7
9 May 2009	NA	NA	123	0.0–0.7 (0.1)	0.2–1.0 (0.4)	3–13 (6)	0.9–3.5 (2.0)	60–70 (70)	8.3	0.1	5.5	83	2.1	1.3	−7.9	0.8
23 Aug 2008	62–46	21–28	60	0.1–2.4 (0.3)	0.4–3.6 (1.7)	8–25 (13)	3.3–8.5 (6.1)	NA	8.2	0.4	8.9	20.5	9.4	2.1	−13.2	0.8
24 Aug 2008	63–54	24–28	0	0.0–1.4 (0.2)	0.3–2.2 (1.4)	9–27 (16)	3.3–4.3 (3.9)	NA	9.1	0.3	8.4	30.3	4.3	1.4	−8.7	0.3
25 Aug 2009	92–43	14–29	135	0.0–0.3 (0.1)	0.3–1.3 (0.7)	12–26 (17)	1.3–18.7 (4.8)	NA	11.7	0.6	13.8	19.5	1.2	1.3	−9.1	0.8
3 Sep 2008	36–34	30–31	30	0.0–1.2 (0.2)	0.6–2.7 (1.6)	16–32 (24)	10.2–13.0 (11.1)	NA	10.3	0.8	15.3	12.9	3.9	2.3	−15.7	0.3
26 Nov 2009[b]	85–49	3–8	39	0.0–0.1 (0.05)	0.0–0.6 (0.1)	1–2 (1.3)	<0.2–0.5 (0.4)	NA	7.2	<0.1	6.8		1.2	1.4	−7.6	0.8
28 Nov 2009	79–44	0–9	74	0.0–0.1 (0.07)	0.0–0.7 (0.4)	1–6 (3.3)	<0.2–3.9 (1.7)	NA	8.3	0.2	8.4	41.5	0.4	0.8	−5.6	0.8

[a] *J* is nucleation rate calculated from PARGAN (that is, J_{PARGAN}), *C* is preexponential factor, and *P* is power, for $J = C[H_2SO_4]^P$. *R* is correlation coefficient of Log *J* versus Log [H_2SO_4] plots.
[b] The ratio of GR_{MODAL} over GR_{H2SO4} for 26 November 2009 was left out because GR_{H2SO4} was close to zero.

the measured *J* was proportional to [H_2SO_4] with the second to tenth powers [*Benson et al.*, 2008]. Other laboratory studies, on the other hand, showed that nucleation takes place at lower [H_2SO_4] concentration [*Berndt et al.*, 2005] and with *J* proportional to [H_2SO_4] to the first to second power [*Metzger et al.*, 2010]. It is unclear at present what causes such discrepancies. While the linear dependence of Log *J* to Log [H_2SO_4] observed in Kent highlights the importance of [H_2SO_4] on NPF, the significant differences in the power dependence of Log *J* to Log [H_2SO_4] and in the [H_2SO_4] threshold value found from laboratory experiments and ambient measurements also indicate that atmospherically observed nucleation events cannot be explained solely by H_2SO_4/H_2O BHN, and it is possible that NH_3 and/or organic compounds likely together play important roles.

5.3. NH_3 Effects on Nucleation

[41] From the simultaneous observations of NH_3 and particles in Kent, we have not seen a clear relationship between J_{PARGAN} and [NH_3] (Figure 7c). This may indicate that NH_3 effects on aerosol nucleation are already saturated at this measured [NH_3] (sub-ppbv), as predicted from modeling studies [*Merikanto et al.*, 2007]. It is also possible that NH_3 is involved in nucleation in much more complex unknown ways. While data in Atlanta suggest a positive association between concentration of particles and [NH_3] [*McMurry et al.*, 2005], [NH_3] in Atlanta were mostly in the 1 to 10 ppbv range, which is about 1 order of magnitude higher than the values in Kent.

[42] We further investigated the role of NH_3 in NPF in Kent, using the current NH_3-THN parameterization model [*Merikanto et al.*, 2007] to predict nucleation rates under the typical measurement conditions. This model provides the relationship of NH_3-THN nucleation rates, J_{THN}, as a function of T, RH, [H_2SO_4] and [NH_3]. When the typical values of our measured T, RH, [H_2SO_4] and [NH_3] were used as input parameters for this parameterization, the model-produced *J* was negligible, indicating that according to this model nucleation cannot take place under the typical atmospheric conditions shown in this study. While this is the most up-to-date model that was constrained by the laboratory observation data [*Ball et al.*, 1999], our results raise concerns on its applicability to ambient data. Further revisions are required to modify the current model to reflect the new observation results. It is also noted that *Benson et al.*'s [2009] recent NH_3-THN studies indicated that under [H_2SO_4] at the 10^9 cm^{-3} range, only very high concentrations of NH_3 (>1 ppbv) can enhance H_2SO_4 nucleation, a different conclusion than that derived by *Ball et al.* [1999]. While we do not understand what causes such differences, our atmospheric observations in Kent seem to agree more with those of *Benson et al.* [2009], although [H_2SO_4] conditions are somewhat different (e.g., 10^7 cm^{-3} seen from ambient conditions versus 10^9 cm^{-3} used in laboratory studies).

5.4. Indirect Chemical Information of Newly Formed Particles

[43] Recent studies have suggested that organic compounds can play a role in nucleation and growth of new particles. For example, theoretical calculations and observations [*Barsanti et al.*, 2009; *Kurten et al.*, 2008; *Smith et al.*, 2008, 2010] have shown that amines may be involved in

aerosol nucleation in the atmosphere. Laboratory studies also showed that aromatic acids may increase nucleation rates similarly to NH_3 [*Zhang et al.*, 2004] and biogenic organic compounds can enhance aerosol growth rates of H_2SO_4 aerosols [*Zhang et al.*, 2009].

[44] The ratios of N_{3-25} measured by the water-CPC versus the butanol-CPC were low (<2) during the period preceding and after nucleation, compared to the onset of nucleation (>20). This implies that during nucleation, the newly formed tiny particles were mainly made up of H_2SO_4, but at the same time other species, likely organic compounds, may also be involved in the growth. This effect of organic compounds in aerosol growth can also be seen from the higher growth rates observed during the summer, when higher concentrations of VOCs from vegetation and their oxidation products are expected owing to warmer temperatures and stronger sunlight.

6. Conclusions

[45] We have measured aerosol size distributions continuously from January 2006 and H_2SO_4 and NH_3 with CIMSs seasonally from August 2008 in Kent, Ohio, for the first time. Particle measurements showed that nucleation took place most frequently in spring and fall and least frequently in winter and summer. This seasonal trend is consistent with those seen in various atmospheric conditions [*Kulmala et al.*, 2004]. [H_2SO_4] showed a clear diurnal variation, lowest during the night and highest at noontime. The median value of noontime peak [H_2SO_4] was higher in spring (5.2×10^6 cm^{-3}) and summer (2.9×10^6 cm^{-3}) and lower in winter (0.6×10^6 cm^{-3}) and fall (0.5×10^6 cm^{-3}). [NH_3] showed no clear daily variation, while it was higher in spring (~300 pptv) than in winter (~70 pptv). J obtained in this study was in the range of 0.4–12.9 cm^{-3}s^{-1}.

[46] Our measured nucleation mode particle concentrations (N_{3-25}) and [H_2SO_4] showed similarities in their diurnal trends; J_{PARGAN} was also proportional to [H_2SO_4] with a power of 0.6 to 2.3. Indirect chemical analysis of newly formed particles derived from the water- and butanol-CPC measurements also suggest that these newly formed particles contain a large fraction of H_2SO_4. These results indicate that H_2SO_4 is an important aerosol nucleation precursor. While numerous THN simulations have shown that nucleation events in the eastern United States can be explained by NH_3 [*Gaydos et al.*, 2005; *Jung et al.*, 2006, 2008; *Stanier et al.*, 2004], our results also show that there is little correlation of J versus [NH_3] at the sub-ppbv range. We have also attempted to apply the current NH_3-THN parameterization [*Merikanto et al.*, 2007] to compare our ambient data but the model predictions did not reproduce observation results of nucleation under the typical measurement conditions. These results imply that the role of NH_3 is not well understood at present and more observations are required to improve the aerosol nucleation theories. The measured GR_{MODAL} and GR_{PARGAN} were both several times higher than the GR_{H2SO4} values calculated from condensation of H_2SO_4, suggesting that other species such as NH_3 and organic compounds are also important for aerosol formation and growth. Furthermore, our GR_{MODAL} were in general highest in summer, while VOC emissions are highest at warm temperatures and with higher photon fluxes. These results imply that organic compounds can be important for aerosol formation, consistent with recent laboratory findings by *Metzger et al.* [2010], *Smith et al.* [2010], and *Zhang et al.* [2009].

[47] While we have attempted to investigate what aerosol nucleation precursors affect the measured nucleation rates and what nucleation mechanisms dominate in our measurement site, it seems that the multicomponent nucleation process involving organic compounds may be involved in this rural environment, as opposed to the BHN or NH_3-THN mechanism alone. It is also possible that even at the same location, depending on the time of the year, different nucleation processes contribute to the particle formation. We have not discussed the roles of ions in aerosol nucleation, as we believe that ion clusters can be important in the upper troposphere and lower stratosphere [*Lee et al.*, 2003] but negligible in the boundary layer [*Eisele et al.*, 2006].

[48] Using an independent approach in a new U.S. continental measurement location which is relatively less polluted than the EPA supersites, we have shown that H_2SO_4 plays an important role in nucleation. Our results have also shown that the role of NH_3 in NPF appears to be more complicated than currently understood. While we did not observe the correlation of nucleation rates to NH_3 mixing ratios at the sub-ppbv level in our rural measurement site mostly because the NH_3 mixing ratios were nearly constant, we do not rule out the NH_3 effects on aerosol nucleation in other atmospheric conditions. This comprehensive and unique data set of seasonal measurements of H_2SO_4, NH_3 and particle size distribution obtained in this new measurement site, together with other NPF studies conducted in different atmospheric environments, can serve as observational basis for testing and improving nucleation theories and further assessing the effects of human-emitted SO_2 and NH_3 on new particle formation and growth.

[49] **Acknowledgments.** S.H.L. gratefully acknowledges funding support from NOAA (NA08OAR4310537), NSF (CAREER ATM-0645567; ATM-0904144), and the Ohio Board of Regents. The authors also thank Greg Huey, David Tanner, and John Nowak for useful discussions and suggestions and acknowledge the NOAA Air Resources Laboratory (ARL) for the provision of the HYSPLIT transport and dispersion model and READY Web site (http://www.arl.noaa.gov/ready.php) used in this publication. FF and VC were NSF chemistry REU students at KSU.

References

Ball, S. M., D. Hanson, F. Eisele, and P. McMurry (1999), Laboratory studies of particle nucleation: Initial results for H_2SO_4, H_2O, and NH_3 vapors, *J. Geophys. Res.*, *104*, 23,709–23,718, doi:10.1029/1999JD900411.

Bardouki, H., et al. (2003), Chemical composition of size-resolved atmospheric aerosols in the eastern Mediterranean during summer and winter, *Atmos. Environ.*, *37*, 195–208, doi:10.1016/S1352-2310(02)00859-2.

Barsanti, K. C., et al. (2009), The potential contribution of organic salts to new particle growth, *Atmos. Chem. Phys.*, *9*, 2949–2957, doi:10.5194/acp-9-2949-2009.

Benson, D. R., L. H. Young, F. R. Kameel, and S.-H. Lee (2008), Laboratory-measured sulfuric acid and water homogeneous nucleation rates from the SO_2 + OH reaction, *Geophys. Res. Lett.*, *35*, L11801, doi:10.1029/2008GL033387.

Benson, D. R., M. E. Erupe, and S.-H. Lee (2009), Laboratory-measured H_2SO_4-H_2O-NH_3 ternary homogeneous nucleation rates: Initial observations, *Geophys. Res. Lett.*, *36*, L15818, doi:10.1029/2009GL038728.

Berndt, T., et al. (2005), Rapid formation of sulfuric acid particles at near-atmospheric conditions, *Science*, *307*, 698–700, doi:10.1126/science.1104054.

Berresheim, H., T. Elste, H. G. Tremmel, A. G. Allen, H.-C. Hansson, K. Rosman, M. Dal Maso, J. M. Mäkelä, M. Kulmala, and C. D. O'Dowd

(2002), Gas-aerosol relationships of H_2SO_4, MSA, and OH: Observations in the coastal marine boundary layer at Mace Head, Ireland, *J. Geophys. Res.*, *107*(D19), 8100, doi:10.1029/2000JD000229.

Birmili, W., A. Wiedensabler, C. Plass-Dülmor, and H. Berresheim (2000), Evolution of newly formed aerosol particles in the continental boundary layer: A case study including OH and H_2SO_4 measurements, *Geophys. Res. Lett.*, *27*, 2205–2208, doi:10.1029/1999GL011334.

Birmili, W., et al. (2003), The Hohenpeissenberg aerosol formation experiments (HAFEX): A long-term study including size-resolved aerosol, H_2SO_4, OH, and monoterpenenes measurements, *Atmos. Chem. Phys.*, *3*, 361–376, doi:10.5194/acp-3-361-2003.

Clarke, A. D., et al. (1998), Particle nucleation in the tropical boundary layer and its coupling to marine sulfur sources, *Science*, *282*, 89–92, doi:10.1126/science.282.5386.89.

Dal Maso, M., et al. (2005), Formation and growth rates of fresh atmospheric aerosols: Eight years of aerosol size distribution data from SMEARII, Hyytiälä, Finland, *Boreal Environ. Res.*, *10*, 323–336.

Eisele, F. L., and D. J. Tanner (1991), Ion-assisted tropospheric OH measurements, *J. Geophys. Res.*, *96*, 9295–9308, doi:10.1029/91JD00198.

Eisele, F. L., and D. J. Tanner (1993), Measurements of gas phase concentrations of H_2SO_4 and methane sulfonic acid and estimates of H_2SO_4 production and loss in the atmosphere, *J. Geophys. Res.*, *98*, 9001–9010, doi:10.1029/93JD00031.

Eisele, F. L., E. R. Lovejoy, E. Kosaiuch, K. F. Moore, R. L. Mauldin, J. N. Smith, P. H. McMurry, and K. Iida (2006), Negative atmospheric ions and their potential role in ion-induced nucleation, *J. Geophys. Res.*, *111*, D04305, doi:10.1029/2005JD006568.

Fiedler, V., et al. (2005), The contribution of sulphuric acid to atmospheric particle formation and growth: A comparison between boundary layers in Northern and Central Europe, *Atmos. Chem. Phys.*, *5*, 1773–1785, doi:10.5194/acp-5-1773-2005.

Friedlander, S. K. (2000), *Smoke, Dust, and Haze: Fundamentals of Aerosol Dynamics*, 2nd ed., Oxford Univ. Press, New York.

Fuchs, N. A., and A. G. Sutugin (1971), Highly dispersed aerosol, in *Topics in Current Aerosol Research*, edited by G. M. Hidy and J. R. Brock, pp. 1–69, Pergamon, New York.

Gaydos, T. M., C. O. Stanier, and S. N. Pandis (2005), Modeling of in situ ultrafine atmospheric particle formation in the eastern United States, *J. Geophys. Res.*, *110*, D07S12, doi:10.1029/2004JD004683.

Gilliland, A. B., R. L. Dennis, S. J. Roselle, and T. E. Pierce (2003), Seasonal NH_3 emission estimates for the eastern United States based on ammonium wet concentrations and an inverse modeling method, *J. Geophys. Res.*, *108*(D15), 4477, doi:10.1029/2002JD003063.

Hanson, D. R., and F. L. Eisele (2000), First measurement of prenucleation molecular clusters, *J. Phys. Chem.*, *104*, 830–836.

Herndon, S. C., et al. (2005), Characterization of urban pollutant emission fluxes and ambient concentration distributions using a mobile laboratory with rapid response instrumentation, *Faraday Discuss.*, *130*, 327–339, doi:10.1039/b500411j.

Huai, T., et al. (2003), Investigation of NH_3 emissions from new technology vehicles as a function of vehicle operating conditions, *Environ. Sci. Technol.*, *37*, 4841–4847, doi:10.1021/es030403+.

Huey, L. G. (2007), Measurement of trace atmospheric species by chemical ionization mass spectrometry: Speciation of reactive nitrogen and recent developments, *Mass Spectrom. Rev.*, *26*, 166–184, doi:10.1002/mas.20118.

Iida, K., M. Stolzenburg, P. McMurry, M. J. Dunn, J. N. Smith, F. Eisele, and P. Keady (2006), Contribution of ion-induced nucleation to new particle formation: Methodology and its application to atmospheric observations in Boulder, Colorado, *J. Geophys. Res.*, *111*, D23201, doi:10.1029/2006JD007167.

Iida, K., M. R. Stolzenburg, P. H. McMurry, and J. N. Smith (2008), Estimating nanoparticle growth rates from size-dependent charged fractions: Analysis of new particle formation events in Mexico City, *J. Geophys. Res.*, *113*, D05207, doi:10.1029/2007JD009260.

Jung, J., et al. (2006), Simulating the size distribution and chemical composition of ultrafine particles during nucleation events, *Atmos. Environ.*, *40*, 2248–2259, doi:10.1016/j.atmosenv.2005.09.082.

Jung, J. G., et al. (2008), Evaluation of nucleation theories in a sulfur-rich environment, *Aerosol Sci. Technol.*, *42*, 495–504, doi:10.1080/02786820802187085.

Kashchiev, D. (1982), On the relation between nucleation work, nucleus size, and nucleation rate, *J. Phys. Chem.*, *76*, 5098–5102, doi:10.1063/1.442808.

Kerminen, V. M., and A. S. Wexler (1996), The occurrence of sulfuric acid-water nucleation in plumes: Urban environment, *Tellus, Ser. B*, *48*, 65–82, doi:10.1034/j.1600-0889.1996.00007.x.

Kiendler-Scharr, A., et al. (2009), New particle formation in forests inhibited by isoprene emissions, *Nature*, *461*(7262), 381–384, doi:10.1038/nature08292.

Kuang, C., P. H. McMurry, A. V. McCormick, and F. L. Eisele (2008), Dependence of nucleation rates on sulfuric acid vapor concentration in diverse atmospheric locations, *J. Geophys. Res.*, *113*, D10209, doi:10.1029/2007JD009253. (Correction, *J. Geophys. Res.*, *115*, D06206, doi:10.1029/2009JD013677, 2010.)

Kulmala, M., and V.-M. Kerminen (2008), On the formation and growth of atmospheric nanoparticles, *Atmos. Res.*, *90*(2–4), 132–150, doi:10.1016/j.atmosres.2008.01.005.

Kulmala, M., et al. (2001a), On the formation, growth, and composition of nucleation mode particles, *Tellus, Ser. B*, *53*, 479–490, doi:10.1034/j.1600-0889.2001.d01-33.x.

Kulmala, M., et al. (2001b), Overview of the international project on biogenic aerosol formation in the boreal forest (BIOFOR), *Tellus, Ser. B*, *53*, 324–343.

Kulmala, M., P. Korhonen, I. Napari, A. Karlsson, H. Berresheim, and C. D. O'Dowd (2002), Aerosol formation during PARFORCE: Ternary nucleation of H_2SO_4, NH_3, and H_2O, *J. Geophys. Res.*, *107*(D19), 8111, doi:10.1029/2001JD000900.

Kulmala, M., et al. (2004), Formation and growth rates of ultrafine atmospheric particles: A review of observations, *J. Aerosol Sci.*, *35*, 143–176, doi:10.1016/j.jaerosci.2003.10.003.

Kulmala, M., et al. (2006), Cluster activation theory as an explanation of the linear dependence between formation rate of 3 nm particles and sulfuric acid concentration, *Atmos. Chem. Phys.*, *6*, 787–793, doi:10.5194/acp-6-787-2006.

Kurten, T., et al. (2008), Amines are likely to enhance neutral and ion-induced sulfuric acid-water nucleation in the atmosphere more effectively than ammonia, *Atmos. Chem. Phys.*, *8*, 4095–4103, doi:10.5194/acp-8-4095-2008.

Lee, S.-H., et al. (2003), Particle formation by ion nucleation in the upper troposphere and lower stratosphere, *Science*, *301*, 1886–1889, doi:10.1126/science.1087236.

Li, Y., J. J. Schwab, and K. L. Demerjian (2006), Measurements of ambient ammonia using a tunable diode laser absorption spectrometer: Characteristics of ambient ammonia emissions in an urban area of New York City, *J. Geophys. Res.*, *111*, D10S02, doi:10.1029/2005JD006275.

Lucas, D. D., and H. Akimoto (2006), Evaluating aerosol nucleation parameterization in a global atmospheric model, *Geophys. Res. Lett.*, *33*, L10808, doi:10.1029/2006GL025672.

Manninen, H., et al. (2009), Charged and total particle formation and growth rates during EUCAARI 2007 campaign in Hyytiälä, *Atmos. Chem. Phys.*, *9*, 4077–4089, doi:10.5194/acp-9-4077-2009.

Marti, J. J., et al. (1997), H_2SO_4 vapor pressure of sulfuric acid and ammonium sulfate solutions, *J. Geophys. Res.*, *102*, 3725–3735, doi:10.1029/96JD03064.

McGraw, R., and R. Zhang (2008), Multivariate analysis of homogeneous nucleation rate measurements: Nucleation in the p-toluic acid/sulfuric acid/water system, *J. Chem. Phys.*, *128*, 064508.

McMurry, P. H., and F. L. Eisele (2005), Preface to topical collection on new particle formation in Atlanta, *J. Geophys. Res.*, *110*, D22S01, doi:10.1029/2005JD006644.

McMurry, P. H., and S. K. Friedlander (1979), New particle formation in the presence of an aerosol, *Atmos. Environ.*, *13*, 1635–1651, doi:10.1016/0004-6981(79)90322-6.

McMurry, P. H., et al. (2005), A criterion for new particle formation in the sulfur-rich Atlanta atmosphere, *J. Geophys. Res.*, *110*, D22S02, doi:10.1029/2005JD005901.

Merikanto, J., I. Napari, H. Vehkamäki, T. Antilla, and M. Kulmala (2007), New parameterization of sulfuric acid-ammonia-water ternary nucleation rates at tropospheric conditions, *J. Geophys. Res.*, *112*, D15207, doi:10.1029/2006JD007977.

Metzger, A., et al. (2010), Evidence for the role of organics in aerosol particle formation under atmospheric conditions, *Proc. Natl. Acad. Sci. U. S. A.*, *107*, 6646–6651.

Napari, I., et al. (2002), An improved model for ternary nucleation of sulfuric acid-ammonia-water, *J. Chem. Phys.*, *116*, 4221–4227, doi:10.1063/1.1450557.

Nieminen, T., et al. (2009), Connection of sulfuric acid to atmospheric nucleation in boreal forest, *Environ. Sci. Technol.*, *43*(13), 4715–4721, doi:10.1021/es803152j.

Nishita, C., K. Osada, M. Kido, K. Matsunaga, and Y. Iwasaka (2008), Nucleation mode particles in upslope valley winds at Mount Norikura, Japan: Implications for the vertical extent of new particle formation events in the lower troposphere, *J. Geophys. Res.*, *113*, D06202, doi:10.1029/2007JD009302.

Nowak, J. B., et al. (2006), Analysis of urban gas phase ammonia measurements from the 2002 Atlanta Aerosol Nucleation and Real-Time Characterization Experiment (ANARChE), *J. Geophys. Res.*, *111*, D17308, doi:10.1029/2006JD007113.

Nowak, J. B., J. A. Nauman, K. Kozai, L. G. Huey, D. J. Tanner, J. S. Holloway, T. B. Ryerson, G. J. Fiost, S. A. McKeen, and F. C. Fehsenfeld (2007), A chemical ionization mass spectrometry technique for airborne measurements of ammonia, *J. Geophys. Res.*, *112*, D10S02, doi:10.1029/2006JD007589.

O'Dowd, C. D., et al. (2002), Coastal new particle formation: Environmental conditions and aerosol physicochemical characteristics during nucleation bursts, *J. Geophys. Res.*, *107*(D19), 8107, doi:10.1029/2000JD000206.

Paasonen, P., et al. (2009), Connection between new particle formation and sulphuric acid at Hohenpeissenberg (Germany) including the influence of organic compounds, *Boreal Environ. Res.*, *14*, 616–629.

Petäjä, T., et al. (2009), Sulfuric acid and OH concentrations in a boreal forest site, *Atmos. Chem. Phys.*, *9*, 7435–7448, doi:10.5194/acp-9-7435-2009.

Riipinen, I., et al. (2007), Connections between atmospheric sulfuric acid and new particle formation during QUEST III–IV campaigns in Heidelberg and Hyytiala, *Atmos. Chem. Phys.*, *7*, 1899–1914, doi:10.5194/acp-7-1899-2007.

Scott, W. D., and F. C. R. Cattell (1979), Vapor pressure of ammonium sulfates, *Atmos. Environ.*, *13*, 307–317, doi:10.1016/0004-6981(79)90174-4.

Seinfeld, J. H., and S. N. Pandis (2006), *Atmospheric Chemistry and Physics: From Air Pollution to Climate Change*, 2nd ed., John Wiley, New York.

Sihto, S.-L., et al. (2006), Atmospheric sulfuric acid and aerosol formation: Implications form atmospheric measurements for nucleation and early growth mechanisms, *Atmos. Chem. Phys.*, *6*, 4079–4091, doi:10.5194/acp-6-4079-2006.

Sihto, S.-L., et al. (2009), Aerosol dynamics simulations on the connection of sulphuric acid and new particle formation, *Atmos. Chem. Phys.*, *9*, 2933–2947, doi:10.5194/acp-9-2933-2009.

Sjostedt, S. J., et al. (2007), Observations of hydroxyl and the sum of peroxy radicals at Summit, Greenland during summer 2003, *Atmos. Environ.*, *41*, 5122–5137, doi:10.1016/j.atmosenv.2006.06.065.

Smith, J. N., K. F. Moore, F. L. Eisele, D. Voisin, A. K. Ghimire, H. Sakurai, and P. H. McMurry (2005), Chemical composition of atmospheric nanoparticles during nucleation in Atlanta, *J. Geophys. Res.*, *110*, D22S03, doi:10.1029/2005JD005912.

Smith, J. N., M. J. Duna, T. M. VanReken, K. Iida, M. R. Stolzenberg, P. H. McMurry, and L. G. Huey (2008), Chemical composition of atmospheric nanoparticles formed from nucleation in Tecamac, Mexico: Evidence for an important role for organic species in nanoparticle growth, *Geophys. Res. Lett.*, *35*, L04808, doi:10.1029/2007GL032523.

Smith, J. N., et al. (2010), Observations of amonium salts in atmospheric nanoparticles and possible climatic implications, *Proc. Natl. Acad. Sci. U. S. A.*, *107*, 6634–6639.

Stanier, C. O., and P. A. Solomon (2006), Preface to special section on Particulate Matter Supersites Program and Related Studies, *J. Geophys. Res.*, *111*, D10S01, doi:10.1029/2006JD007381.

Stanier, C. O., et al. (2004), Nucleation events during the Pittsburgh air quality study: Description and relation to key meteorological, gas phase, and aerosol parameters, *Aerosol Sci. Technol.*, *38*, 253–264, doi:10.1080/02786820390229570.

Stolzenberg, M. R., P. H. McMurry, H. Sakurai, J. N. Smith, R. J. Mauldin, F. L. Eisele, and C. F. Clement (2005), Growth rates of freshly nucleated atmospheric particles in Atlanta, *J. Geophys. Res.*, *110*, D22S05, doi:10.1029/2005JD005935.

Tanner, D. J., and F. L. Eisele (1995), Present OH measurement limits and associated uncertainties, *J. Geophys. Res.*, *100*, 2883–2892, doi:10.1029/94JD02609.

Verheggen, B. (2004), Determination of particle nucleation and growth rates from measured aerosol size distributions, Ph.D. thesis, Dep. of Chem., York Univ., Toronto, Ont., Canada.

Verheggen, B., and M. Mozurkewich (2002), Determination of nucleation and growth rates from observation of a SO_2 induced atmospheric nucleation event, *J. Geophys. Res.*, *107*(D11), 4123, doi:10.1029/2001JD000683.

Verheggen, B., and M. Mozurkewich (2006), An inverse modeling procedure to determine particle growth and nucleation rates from measured aerosol size distributions, *Atmos. Chem. Phys.*, *6*, 2927–2942, doi:10.5194/acp-6-2927-2006.

Viggiano, A. A., R. A. Perry, D. L. Albritton, E. Ferguson, and F. Fehsenfeld (1982), Stratospheric negative-ion reaction rates with H_2SO_4, *J. Geophys. Res.*, *87*, 7340–7342, doi:10.1029/JC087iC09p07340.

Viggiano, A. A., et al. (1997), Rate constants for the reactions of $XO_3^-(H_2O)_n$ (X = C, HC, and N) and $NO_3^-(HNO_3)_n$ with H_2SO_4: Implications for atmospheric detection of H_2SO_4, *J. Phys. Chem. A*, *101*, 8275–8278, doi:10.1021/jp971768h.

Weber, R. J., et al. (1996), Measured atmospheric new particle formation rates: Implications for nucleation mechanisms, *Chem. Eng. Commun.*, *151*, 53–64, doi:10.1080/00986449608936541.

Weber, R. J., J. Marti, P. McMurry, F. Eisele, D. Tanner, and A. Jefferson (1997), Measurements of new particle formation and ultrafine particle growth rates at a clean continental site, *J. Geophys. Res.*, *102*, 4375–4385, doi:10.1029/96JD03656.

Weber, R. J., P. H. McMurry, L. Mauldin, D. J. Tanner, F. L. Eisele, F. J. Brechtel, S. M. Kreidenweis, G. L. Kok, R. D. Schillawski, and D. Baumgardner (1998), A study of new particle formation and growth involving biogenic and trace gas species measured during ACE 1, *J. Geophys. Res.*, *103*, 16,385–16,396, doi:10.1029/97JD02465.

Weber, R. J., P. H. McMurry, R. L. Mauldin, D. J. Tanner, F. L. Eisele, A. D. Clarke, and V. N. Kapustin (1999), New particle formation in the remote troposphere: A comparison of observations at various sites, *Geophys. Res. Lett.*, *26*, 307–310, doi:10.1029/1998GL900308.

Young, L. H., et al. (2008), Laboratory studies of sulfuric acid and water binary homogeneous nucleation: Evaluation of laboratory setup and preliminary results, *Atmos. Chem. Phys.*, *8*, 1–20.

Zhang, R., et al. (2004), Atmospheric new particle formation enhanced by organic acids, *Science*, *304*, 1487–1490, doi:10.1126/science.1095139.

Zhang, R., et al. (2009), Formation of nanoparticles of blue haze enhanced by anthropogenic pollution, *Proc. Natl. Acad. Sci. U. S. A.*, *106*(42), 17,650–17,654, doi:10.1073/pnas.0910125106.

M. Al-Refai, D. R. Benson, V. Cunningham, M. E. Erupe, F. Frimpong, S.-H. Lee, J. Li, O. Tahboub, and L.-H. Young, Department of Chemistry, Kent State University, Kent, OH 44240, USA. (slee19@kent.edu)

B. Verheggen, Department of Air Quality and Climate Change, Energy Research Centre of the Netherlands, NL-1755 ZG Petten, Netherlands.

A. A. Viggiano, Air Force Research Laboratory, Hanscom Air Force Base, Bedford, MA 01730, USA.